BRCA1^{185delAG} tumors may acquire therapy resistance through expression of RING-less BRCA1

Rinske Drost,[1] Kiranjit K. Dhillon,[2] Hanneke van der Gulden,[1] Ingrid van der Heijden,[1] Inger Brandsma,[3] Cristina Cruz,[4,5] Dafni Chondronasiou,[1] Marta Castroviejo-Bermejo,[4] Ute Boon,[1] Eva Schut,[1] Eline van der Burg,[1] Ellen Wientjens,[1] Mark Pieterse,[1] Christiaan Klijn,[1] Sjoerd Klarenbeek,[1] Fabricio Loayza-Puch,[6] Ran Elkon,[6] Liesbeth van Deemter,[1] Sven Rottenberg,[1,7] Marieke van de Ven,[8] Dick H.W. Dekkers,[9] Jeroen A.A. Demmers,[9] Dik C. van Gent,[3] Reuven Agami,[6] Judith Balmaña,[5] Violeta Serra,[4] Toshiyasu Taniguchi,[2] Peter Bouwman,[1] and Jos Jonkers[1]

[1]Division of Molecular Pathology and Cancer Genomics Netherlands, The Netherlands Cancer Institute, Amsterdam, The Netherlands. [2]Divisions of Human Biology and Public Health Sciences, Fred Hutchinson Cancer Research Center, Seattle, Washington, USA. [3]Department of Genetics, Erasmus University Medical Center, Rotterdam, The Netherlands. [4]Experimental Therapeutics Group and [5]High Risk and Cancer Prevention Group, Medical Oncology Department, Vall d'Hebron University Hospital and Vall d'Hebron Institute of Oncology, Barcelona, Spain. [6]Division of Biological Stress Response, The Netherlands Cancer Institute, Amsterdam, The Netherlands. [7]Institute of Animal Pathology, Vetsuisse Faculty, University of Bern, Bern, Switzerland. [8]Preclinical Intervention Unit, Mouse Cancer Clinic, The Netherlands Cancer Institute, Amsterdam, The Netherlands. [9]Proteomics Center, Erasmus University Medical Center, Rotterdam, The Netherlands.

Heterozygous germline mutations in breast cancer 1 (*BRCA1*) strongly predispose women to breast cancer. BRCA1 plays an important role in DNA double-strand break (DSB) repair via homologous recombination (HR), which is important for tumor suppression. Although BRCA1-deficient cells are highly sensitive to treatment with DSB-inducing agents through their HR deficiency (HRD), *BRCA1*-associated tumors display heterogeneous responses to platinum drugs and poly(ADP-ribose) polymerase (PARP) inhibitors in clinical trials. It is unclear whether all pathogenic *BRCA1* mutations have similar effects on the response to therapy. Here, we have investigated mammary tumorigenesis and therapy sensitivity in mice carrying the *Brca1*^{185stop} and *Brca1*^{5382stop} alleles, which respectively mimic the 2 most common *BRCA1* founder mutations, *BRCA1*^{185delAG} and *BRCA1*^{5382insC}. Both the *Brca1*^{185stop} and *Brca1*^{5382stop} mutations predisposed animals to mammary tumors, but *Brca1*^{185stop} tumors responded markedly worse to HRD-targeted therapy than did *Brca1*^{5382stop} tumors. Mice expressing *Brca1*^{185stop} mutations also developed therapy resistance more rapidly than did mice expressing *Brca1*^{5382stop}. We determined that both murine *Brca1*^{185stop} tumors and human *BRCA1*^{185delAG} breast cancer cells expressed a really interesting new gene domain–less (RING-less) BRCA1 protein that mediated resistance to HRD-targeted therapies. Together, these results suggest that expression of RING-less BRCA1 may serve as a marker to predict poor response to DSB-inducing therapy in human cancer patients.

Introduction

Breast cancer is one of the most common malignancies in women, accounting for almost 1 in 3 diagnosed cancers, and it is the second leading cause of cancer death among women in Western countries (1). Five percent to ten percent of all breast cancer cases have a hereditary component, and thirty percent to eighty percent of all hereditary cases are attributable to mutations in the breast cancer 1 or breast cancer 2 (*BRCA1* or *BRCA2*) gene. Germline mutations in the *BRCA1* gene predispose women to hereditary breast and ovarian cancer (HBOC), with an 80%–90% lifetime risk of developing breast cancer and a 40%–50% risk of developing ovarian cancer (2).

Germline *BRCA1* mutations are scattered throughout the 81-kb-long gene that encompasses 22 coding exons (3). Most of the known pathogenic *BRCA1* mutations are predicted to result in premature termination of protein translation and nonsense-mediated mRNA decay (NMD) (4, 5). These mutations include small deletions and insertions that generate frameshifts, single-base substitutions that produce termination codons, and splice site errors (2). Although there are many different *BRCA1* mutations, in certain ethnic populations, only a few founder mutations account for almost all *BRCA1*-associated breast and/or ovarian cancer families. Two founder mutations, *BRCA1*^{185delAG} and *BRCA1*^{5382insC}, account for the vast majority of *BRCA1* mutations in the Ashkenazi Jewish population (2, 6). The *BRCA1*^{185delAG} and *BRCA1*^{5382insC} mutations are carried, respectively, by 1% and 0.15% of Ashkenazi Jews (7, 8). The prevalence of these mutations in unselected patients of Ashkenazi Jewish ethnicity who have ovarian cancer was found to be close to 30% and may even exceed 50% in patients with a family history of breast and/or ovarian cancer (9–11).

BRCA1 has been implicated in various cellular processes, including DNA repair, cell-cycle control, and transcriptional regulation (12). In particular, the role of BRCA1 in homologous recombination–mediated (HR-mediated) repair of DNA double-strand breaks (DSBs) appears to be important in the maintenance of genomic stability and tumor suppression (13). Impaired HR also renders BRCA1-deficient cells extremely sensitive to DSB-inducing agents, like platinum drugs (14). In line with this, patients

▶ Related Commentary: p. 2802

Conflict of interest: The authors have declared that no conflict of interest exists.
Submitted: March 29, 2013; **Accepted:** May 9, 2016.
Reference information: *J Clin Invest*. 2016;126(8):2903–2918. doi:10.1172/JCI70196.

with *BRCA1*-mutated ovarian cancer had a better prognosis after platinum-based chemotherapy than did nonmutation carriers (15–18). More recently, it was also shown that triple-negative breast cancers in *BRCA1* mutation carriers were highly sensitive to neoadjuvant cisplatin chemotherapy (19). Moreover, patients harboring breast tumors with a BRCA1-like genomic profile had a significantly greater benefit from high-dose, platinum-based chemotherapy versus conventional chemotherapy than did patients with non-BRCA1–like tumors (20). Also, chemical inhibitors of poly(ADP-ribose) polymerase (PARP), an enzyme involved in DNA single-strand break (SSB) repair, are effective against BRCA-deficient tumors in preclinical models (21–23) and in patients carrying *BRCA* mutations (24–29). Recently, the clinical PARP inhibitor olaparib (Lynparza) has been approved as maintenance therapy for *BRCA* mutation carriers with platinum-sensitive ovarian cancer (30). PARP inhibition results in an increased number of DSBs due to replication fork collapse at SSBs. PARP inhibition is therefore selectively toxic in cells that lack HR-mediated DSB repair, such as BRCA1/2-deficient tumor cells.

The *BRCA1* gene encodes for a protein of 1863 aa that contains a highly conserved amino-terminal really interesting new gene (RING) domain and tandem BRCA1 C-terminus domain (BRCT) repeats at its carboxyl terminus (31). The RING domain of BRCA1 is required for stable interaction with BRCA1-associated RING domain 1 (BARD1), and the BRCA1/BARD1 heterodimer has E3 ubiquitin ligase activity with the class of UBCH5 E2 ubiquitin–conjugating enzymes (32, 33). The observation that BRCA1/BARD1-dependent ubiquitin conjugates occur at DSBs suggests that the BRCA1/BARD1 heterodimer is important for DNA repair and thereby for the tumor-suppressive function of BRCA1 (34). BRCA1 has been reported to interact with numerous other proteins involved in DNA repair, cell-cycle checkpoint control, transcription, and chromatin remodeling, mainly through its BRCT domains (35–40).

Recent studies have shown that not all biochemical activities of BRCA1 are equally important for its role in tumor suppression and therapy response (41). Using genetically engineered mouse models, Shakya and coworkers showed that loss of BRCA1 E3 ligase activity does not lead to tumor formation, while loss of BRCT phosphoprotein binding does (42). We showed that BRCA1 RING function is essential for tumor suppression, but does not lead to hypersensitivity to homologous recombination deficiency–targeting (HRD-targeting therapy (43). Mouse mammary tumors that express a mutant BRCA1-C61G protein, which lacks a functional RING domain, respond much worse to DSB-inducing therapy than do *Brca1*-null tumors. In addition, tumors carrying the $Brca1^{C61G}$ mutation rapidly develop therapy resistance, while retaining the *Brca1* mutation. These data suggest that the mutant BRCA1-C61G protein has some residual activity in the DNA damage response. This may not only hold true for the $BRCA1^{C61G}$ missense mutation, but also for other *BRCA1* mutations, and could indicate the existence of differences in therapeutic response and resistance between different *BRCA1* mutation carriers.

In the present study, we investigated the effects of the 2 most common *BRCA1* frameshift mutations, $BRCA1^{185delAG}$ and $BRCA1^{5382insC}$, on tumor development and therapy response and resistance in genetically engineered mouse models.

Results

Generation of $Brca1^{185stop}$ *and* $Brca1^{5382stop}$ *alleles*. In order to mimic the human $BRCA1^{185delAG}$ and $BRCA1^{5382insC}$ mutations in mice, we used short, synthetic, single-stranded oligodeoxyribonucleotides to introduce mutations into the genome of mouse embryonic stem cells (mESCs). It has previously been shown that this technique requires (transient) suppression of DNA mismatch repair (MMR) by knockdown of *Mlh1* or knockout of *Msh2* or *Msh3* (44–47). In order to mimic the $BRCA1^{185delAG}$ mutation, we introduced the $Brca1^{185stop}$ mutation into *Mlh1*-knockdown mESCs by substitution of 3 nucleotides (TCC to AAG), thereby creating an early STOP codon at aa 24 (Figure 1A). We used *Msh3*-knockout mESCs to insert 4 nucleotides (AGGA) to generate the $Brca1^{5382stop}$ mutation, which resulted in premature protein truncation at aa 1713 and closely resembled the human $BRCA1^{5382insC}$ mutation (Figure 1B). $Brca1^{185stop}$ and $Brca1^{5382stop}$ mutant mESCs were injected into 3.5-day-old C57BL/6J blastocysts to generate chimeric mice. Chimeric mice were mated with FVB female mice, and germline transmission of the mutant alleles was verified by melting-curve genotyping, PCR, and sequencing (Figure 1, C and D, and data not shown).

Embryonic lethality of homozygous $Brca1^{185stop}$ *and* $Brca1^{5382stop}$ *mice*. To determine the effect of the $Brca1^{185stop}$ and $Brca1^{5382stop}$ mutations on normal mouse development, we intercrossed heterozygous $Brca1^{185stop}$ or $Brca1^{5382stop}$ mice to produce homozygous offspring. No homozygous pups were born (Supplemental Table 1; supplemental material available online with this article; doi:10.1172/JCI70196DS1), indicating that homozygous $Brca1^{185stop}$ or $Brca1^{5382stop}$ mutations lead to embryonic lethality. To study at which stage of embryonic development homozygous $Brca1^{185stop}$ and $Brca1^{5382stop}$ mice die, embryos were harvested and genotyped at several time points after gestation. Although (resorbed) homozygous $Brca1^{185stop}$ and $Brca1^{5382stop}$ embryos could still be recovered from E12.5 to E13.5 (Supplemental Table 1), they were already severely delayed in development at E9.5 compared with WT and heterozygous embryos (Figure 1, E and F).

Mammary tumor development in K14-Cre $Brca1^{fl/185stop}$ $p53^{fl/fl}$ *and K14-Cre* $Brca1^{fl/5382stop}$ $p53^{fl/fl}$ *mice*. To investigate the influence of $Brca1^{185stop}$ and $Brca1^{5382stop}$ mutations on tumor development, we independently introduced both alleles into the *K14-Cre* $Brca1^{fl/fl}$ $p53^{fl/fl}$ mouse model (referred to hereafter as *KB1P* mice), in which epithelium-specific deletion of $Brca1^{fl}$ and $p53^{fl}$ alleles predisposes mice to mammary and skin tumor formation (48). The resulting mice carry 1 $Brca1^{185stop}$ or 1 $Brca1^{5382stop}$ allele throughout their body and sporadically lose the remaining *Brca1* WT allele in specific tissues, including mammary gland. We crossed heterozygous $Brca1^{185stop}$ and $Brca1^{5382stop}$ mice with *KB1P* animals to generate cohorts of *K14-Cre* $Brca1^{fl/185stop}$ $p53^{fl/fl}$ mice [referred to hereafter as *KB1(185stop)P* mice], *K14-Cre* $Brca1^{fl/5382stop}$ $p53^{fl/fl}$ [referred to hereafter as *KB1(5382stop)P* mice], and *KB1P* littermate controls. The 3 cohorts were monitored for spontaneous tumor formation and showed equal rates of tumor-free survival (TFS) (Figure 2A). For all cohorts, the median TFS was approximately 200 days, which is similar to what has been described previously for *KB1P* mice (48) and for mice carrying the $Brca1^{C61G}$ mutation (43). In addition, no obvious differences in TFS could be detected between cohorts when only mammary tumors (Figure 2B) or skin tumors (Supplemental Figure 1A) were taken into account. Mammary and

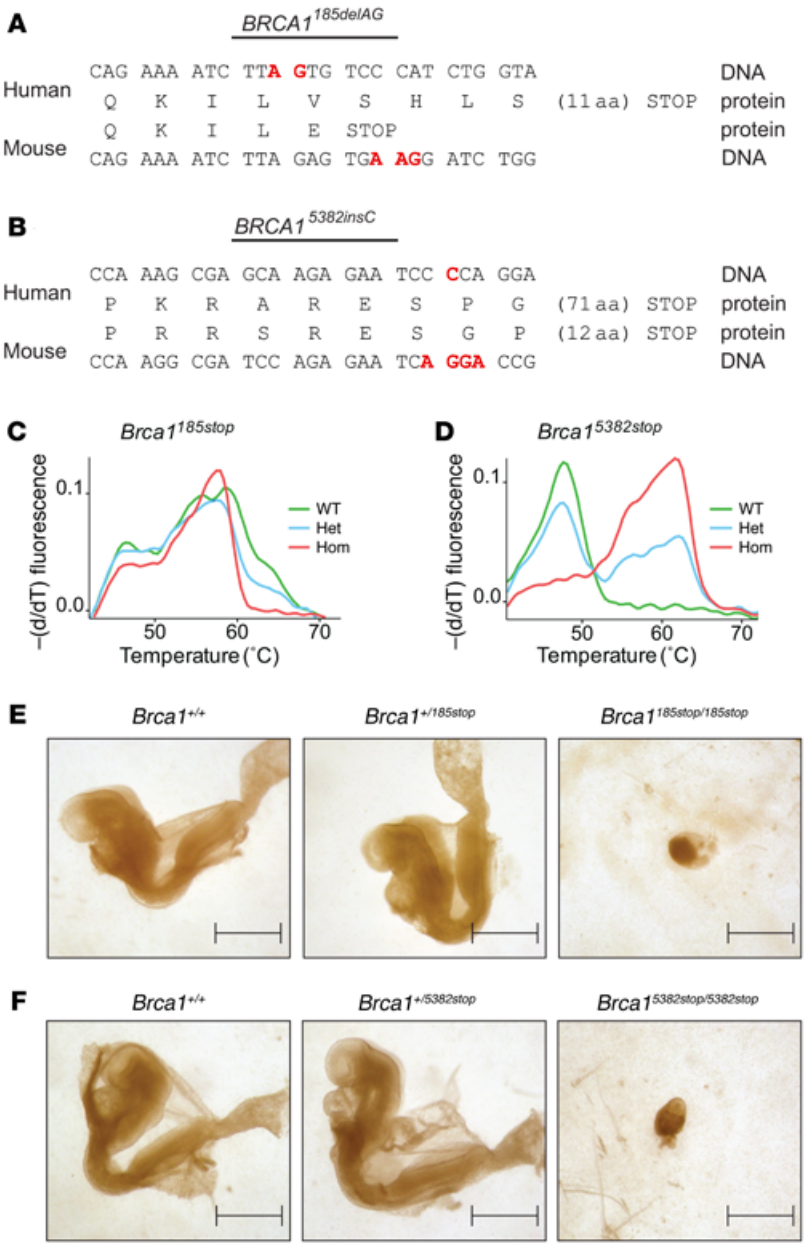

Figure 1. Characterization of *Brca1*-mutant alleles. (**A**) DNA sequences and protein translations for the human *BRCA1*^{185delAG} and mouse *Brca1*^{185stop} mutations. Mutations are indicated in red. The number of aa until the STOP codon is indicated in parentheses. (**B**) DNA sequences and protein translations for the human *BRCA1*^{5382insC} and mouse *Brca1*^{5382stop} mutations. (**C**) Melting-curve genotyping of *Brca1*^{185stop}-mutant mice. WT, *Brca1*$^{+/+}$; Het, *Brca1*$^{+/185stop}$; and Hom, *Brca1*$^{185stop/185stop}$. (**D**) Melting-curve genotyping of *Brca1*^{5382stop}-mutant mice. WT, *Brca1*$^{+/+}$; Het, *Brca1*$^{+/5382stop}$, and Hom, *Brca1*$^{5382stop/5382stop}$. Data in **C** and **D** are plotted as the first negative derivative of the sample fluorescence versus temperature [−(d/dT)]. (**E**) Embryonic lethality of homozygous *Brca1*^{185stop} mice. Images of *Brca1*$^{+/+}$, *Brca1*$^{185stop/+}$, and *Brca1*$^{185stop/185stop}$ embryos at E9.5. Scale bars: 1 mm. (**F**) Embryonic lethality of homozygous *Brca1*^{5382stop} mice. Images of *Brca1*$^{+/+}$, *Brca1*$^{+/5382stop}$, and *Brca1*$^{5382stop/5382stop}$ embryos at E9.5. Het, heterozygous; Hom, homozygous.

skin TFS rates were comparable between *KB1P* mice derived from the 185delAG cohort and from the 5382insC cohort (Supplemental Figure 1, B and C). Furthermore, the spectrum and incidence of tumors that developed were similar among *KB1(185stop)P*, *KB1(5382stop)P*, and *KB1P* mice (Supplemental Figure 1D).

Characterization of KB1(185stop)P and KB1(5382stop)P mammary tumors. On the basis of their histomorphological characteristics, the majority of mammary tumors that developed in *KB1(185stop)P* (84%), *KB1(5382stop)P* (79%), and *KB1P* mice (85%) were classified as poorly differentiated, solid carcinomas (Figure 2C and Supplemental Figure 1, E and F). In line with this observation, most *KB1(185stop)P* and *KB1(5382stop)P* mammary tumors stained (partially) positive for the epithelial marker cytokeratin 8 and negative for the mesenchymal marker vimentin (Supplemental Figure 1, G and H, and Supplemental Table 2). In all cohorts, only a small fraction of mammary tumors (8%) was classified as carcinosarcoma, characterized by the presence of spindle-shaped cells (Figure 2C and Supplemental Figure 1, E and F). Other mammary tumors that developed in *KB1(185stop)P*, *KB1(5382stop)P*, and *KB1P* mice were grouped as lumen-forming carcinomas with varying degrees of glandular differentiation (Figure 2C and Supplemental Figure 1, E and F). Like the majority of human *BRCA1*–mutated breast cancers (49), most *KB1(185stop)P* and *KB1(5382stop)P* mammary tumors stained negative for the estrogen receptor (Supplemental Figure 1, G and H, and Supplemental Table 2).

A high level of genomic instability is one of the hallmarks of human *BRCA1*–associated breast cancer (50), and BRCA1-deficient mouse mammary tumors display a considerably larger number of genetic aberrations than do BRCA1-proficient tumors (43, 48, 51). To investigate the level of genomic instability in *KB1(185stop)P* and *KB1(5382stop)P* tumors, we measured DNA copy number aberrations (CNAs) in mammary tumors from *KB1(185stop)P* (n = 20),

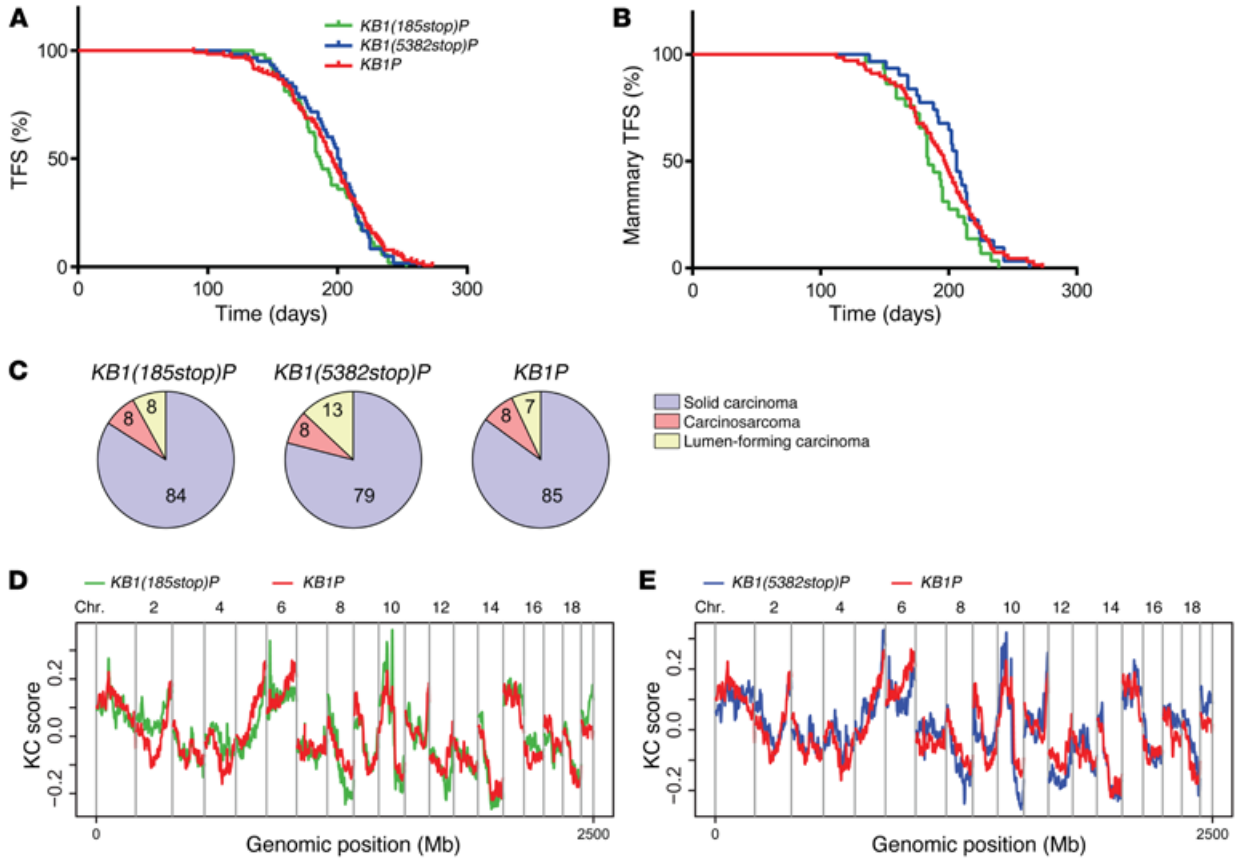

Figure 2. Development of genomically unstable mammary tumors in mice carrying *Brca1*^{185stop} or *Brca1*^{5382stop} mutations. (**A**) TFS curves of *KB1(185stop)P* (n = 53, t_{50} = 186 days), *KB1(5382stop)P* (n = 60, t_{50} = 200 days) and *KB1P* (n = 128, t_{50} = 196 days) mice. P = 0.4510 (NS), by log-rank test for *KB1(185stop)P* versus *KB1(5382stop)P*. (**B**) Mammary TFS curves of *KB1(185stop)P* (n = 29, t_{50} = 184 days), *KB1(5382stop)P* (n = 31, t_{50} = 206 days), and *KB1P* (n = 68, t_{50} = 197 days). P = 0.0415 (NS), by log-rank test for *KB1(185stop)P* versus *KB1(5382stop)P*. (**C**) Distribution of mammary tumor types in *KB1(185stop)P*, *KB1(5382stop)P*, and *KB1P* mice. Numbers in the pie chart represent percentages. (**D**) Comparative KCsmart (KC) profiles of *KB1(185stop)P* and *KB1P* mouse mammary tumors. (**E**) Comparative KCsmart profiles of *KB1(5382stop)P* and *KB1P* tumors. t_{50}, median survival; n, number of mice; Chr., chromosome.

KB1(5382stop)P (n = 20), and littermate control *KB1P* mice (n = 22) using array comparative genomic hybridization (aCGH). When applying the comparative module of the R package KCsmart (52, 53), we did not detect any differences between recurrent CNAs in *KB1(185stop)P* or *KB1P* tumors (Figure 2D). We also could not find any differences in recurrent CNAs between *KB1(5382stop)P* and *KB1P* tumors (Figure 2E). On the basis of these results, we conclude that the histological and genetic features of *KB1(185stop)P* and *KB1(5382stop)P* mammary tumors are indistinguishable from each other and from those of *KB1P* control tumors.

Response of KB1(185stop)P mammary tumors to the PARP inhibitor olaparib. PARP inhibitors have been shown to be effective in breast and ovarian cancer patients carrying *BRCA1/2* mutations (24–28). To study the response of *KB1(185stop)P* and *KB1(5382stop)P* tumors to PARP inhibition, we transplanted several independent *KB1(185stop)P*, *KB1(5382stop)P*, BRCA1-deficient *KB1P*, and BRCA1-proficient *K14-Cre p53*$^{fl/fl}$ (referred to hereafter as *KP*) tumors into the fourth mammary gland of syngeneic female recipient mice. This orthotopic transplantation model ensures that transplanted mouse mammary tumors retain the histomorphological features, molecular characteristics, and drug-sensitivity profiles of their spontaneous counterparts (54, 55). When tumors reached a volume of 200 mm^3, tumor-bearing mice were treated with 50 mg/kg of the PARP inhibitor olaparib (AZD2281) for 28 consecutive days or left untreated (Figure 3A).

We did not observe any differences in overall survival (OS) between mice that did not receive treatment; all mice had to be sacrificed within 25 days because of a large tumor (Figure 3B and Supplemental Figure 2). The *KP* and *KB1P* data have been published before (43). While mice carrying *KP* tumors did not respond at all to olaparib treatment (Figure 3, C and D; black curves; median OS [t_{50}] = 10 days), the median OS of mice carrying *KB1P* tumors increased from 12 to 60 days following olaparib treatment, and their tumors disappeared completely during the course of treatment (Figure 3, C and D; red curves). However, *KB1P* tumors could not be fully eradicated with this 28-day olaparib dosing schedule, and tumors reappeared after the end of the treatment period.

The median OS of mice transplanted with *KB1(5382stop)P* tumors increased from 8 to 52 days after olaparib treatment (Figure 3, B and C; blue curves), which was significantly better than the median OS of mice transplanted with *KP* tumors [*KB1(5382stop)P* vs. *KP*, $P < 0.0001$, log-rank test]. No significant difference in OS was observed between mice with *KB1(5382stop)P* tumors and those

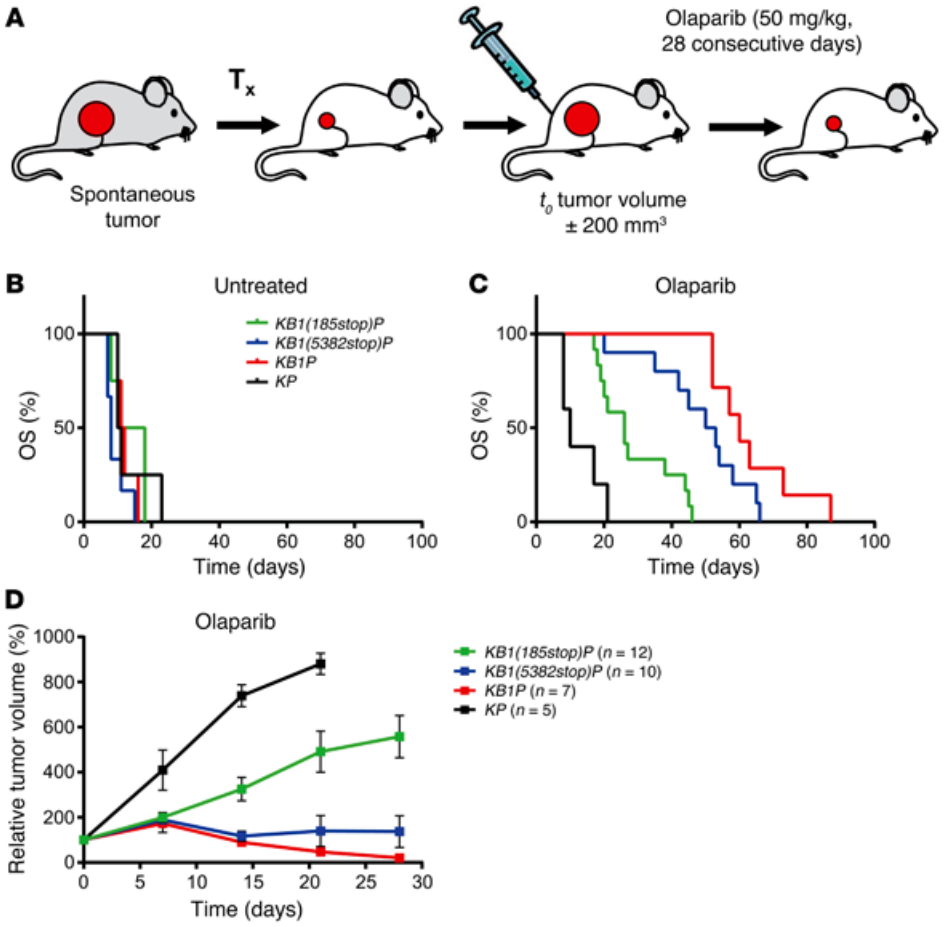

Figure 3. Poor olaparib response of *KB1(185stop)P* mouse mammary tumors. (**A**) Schematic representation of olaparib treatment schedule. T_x, orthotopic transplantation of fragments from spontaneous mouse mammary tumors; t_0, start of treatment at a tumor volume of 200 mm³ (100%). Mice received a daily dose of 50 mg/kg olaparib i.p. for 28 consecutive days. (**B**) OS curves of mice transplanted with *KB1(185stop)P*, *KB1(5382stop)P*, *KB1P*, or *KP* tumors without treatment. t_{50}, median OS. *KB1(185stop)P*: t_{50} = 15 days, n = 4 mice; *KB1(5382stop)P*: t_{50} = 8 days, n = 6 mice; *KB1P*: t_{50} = 12 days, n = 4 mice; *KP*: t_{50} = 11 days, n = 4 mice. (**C**) OS curves of mice transplanted as indicated in **B**, after olaparib treatment. *KB1(185stop)P*: t_{50} = 26 days, n = 12 mice; *KB1(5382stop)P*: t_{50} = 52 days, n = 10 mice; *KB1P*: t_{50} = 60 days, n = 7 mice; *KP*: t_{50} = 10 days, n = 5 mice. P = 0.0012, by log-rank test for *KB1(185stop)P* vs. *KB1(5382stop)P*; $P < 0.0001$, by log-rank test for *KB1(185stop)P* vs. *KB1P*; P = 0.0017, log-rank test for *KB1(185stop)P* vs. *KP*; P = 0.0905 (NS), by log-rank test for *KB1(5382stop)P* vs. *KB1P*; $P < 0.0001$, by log-rank test for *KB1(5382stop)P* vs. *KP*; and P = 0.0003, by log-rank test for *KB1P* vs. *KP*. (**D**) Comparison of relative mammary tumor volumes during a 28-day treatment with olaparib. Tumor volumes are relative to the tumor volume at the start of treatment (day 0, 100% = ±200 mm³). Error bars indicate SEM.

with *KB1P* tumors after treatment with olaparib [*KB1(5382stop)P* vs. *KB1P*, P = 0.0905 (NS), log-rank test]. However, in contrast to *KB1P* tumors, *KB1(5382stop)P* tumors never completely disappeared during olaparib treatment, but rather entered a phase of tumor stasis (Figure 3D; blue curve).

Interestingly, mice transplanted with *KB1(185stop)P* tumors had a median OS of 26 days after the start of olaparib treatment (Figure 3C; green curve), which was significantly better than for mice with BRCA1-proficient *KP* tumors [*KB1(185stop)P* vs. *KP*, P = 0.0017, log-rank test], but significantly worse than for mice with BRCA1-deficient *KB1P* tumors [*KB1(185stop)P* vs. *KB1P*, $P < 0.0001$, log-rank test]. While *KB1(185stop)P* tumors kept growing during the course of olaparib treatment, their growth rate was reduced compared with that of *KP* tumors (Figure 3D; green curve). Moreover, the olaparib response of *KB1(185stop)P* tumors was markedly worse than the response of *KB1(5382stop)P* tumors [Figure 3, C and D and Supplemental Figure 2; *KB1(185stop)P* vs. *KB1(5382stop)P*, P = 0.0012, log-rank test]. The response of *KB1(185stop)P* tumors to olaparib treatment closely resembled the response of *K14-Cre Brca1*$^{fl/C61G}$ *p53*$^{fl/fl}$ (referred to hereafter as *KB1C61GP*) mouse mammary tumors to olaparib (43).

Response of KB1(185stop)P mammary tumors to cisplatin. Since *BRCA1*-associated tumors are also known to be sensitive to platinum drugs (56), we transplanted several *KB1(185stop)P*, *KB1(5382stop)P*, *KB1P*, and BRCA1-proficient *KP* mammary tumors to study potential differences in their response to cisplatin (Supplemental Table 3). Tumor-bearing mice were injected with the maximal tolerable dose of cisplatin and re-treated every 2 weeks when the tumor volume was more than 50% of the starting volume. If the tumor size after 2 weeks was smaller than 50%, treatment was postponed until the tumor reached 100% of the starting volume (Figure 4A). As some animals had to be sacrificed because of the toxic side effects of multiple cisplatin doses, we measured OS as well as TFS rates. Again, the data on the *KP* and *KB1P* controls have been previously published (43).

The median OS of mice transplanted with *KB1(5382stop)P* tumors was prolonged from 8 to 159 days after cisplatin treatment (Figure 4, B and C; blue curves), which is identical to the response of mice transplanted with BRCA1-deficient *KB1P* tumors (43) [Figure 4, B and C; red curves, *KB1(5382stop)P* vs. *KB1P*; P = 0.9696 (NS), log-rank test]. Almost all mice transplanted with *KB1(5382stop)P* tumors had to be sacrificed because of cisplatin toxicity and not because of therapy resistance (Figure 4D). In contrast, the median OS of mice transplanted with *KB1(185stop)P* mammary tumors was only prolonged from 15 to 55 days after treatment with cisplatin (Figure 4, B and C; green curves) and was indistinguishable from the response of BRCA1-proficient tumors [Figure 4, B and C; black curves, *KB1(185stop)P* vs. *KP*, P = 0.2550 (NS), log-rank test]. After an initial response to cisplatin, *KB1(185stop)P* tumors rapidly acquired resistance, and 62% of the mice needed to be sacrificed because of therapy-resistant tumors (Figure 4D). Remarkably, the response of *KB1(185stop)P* tumors

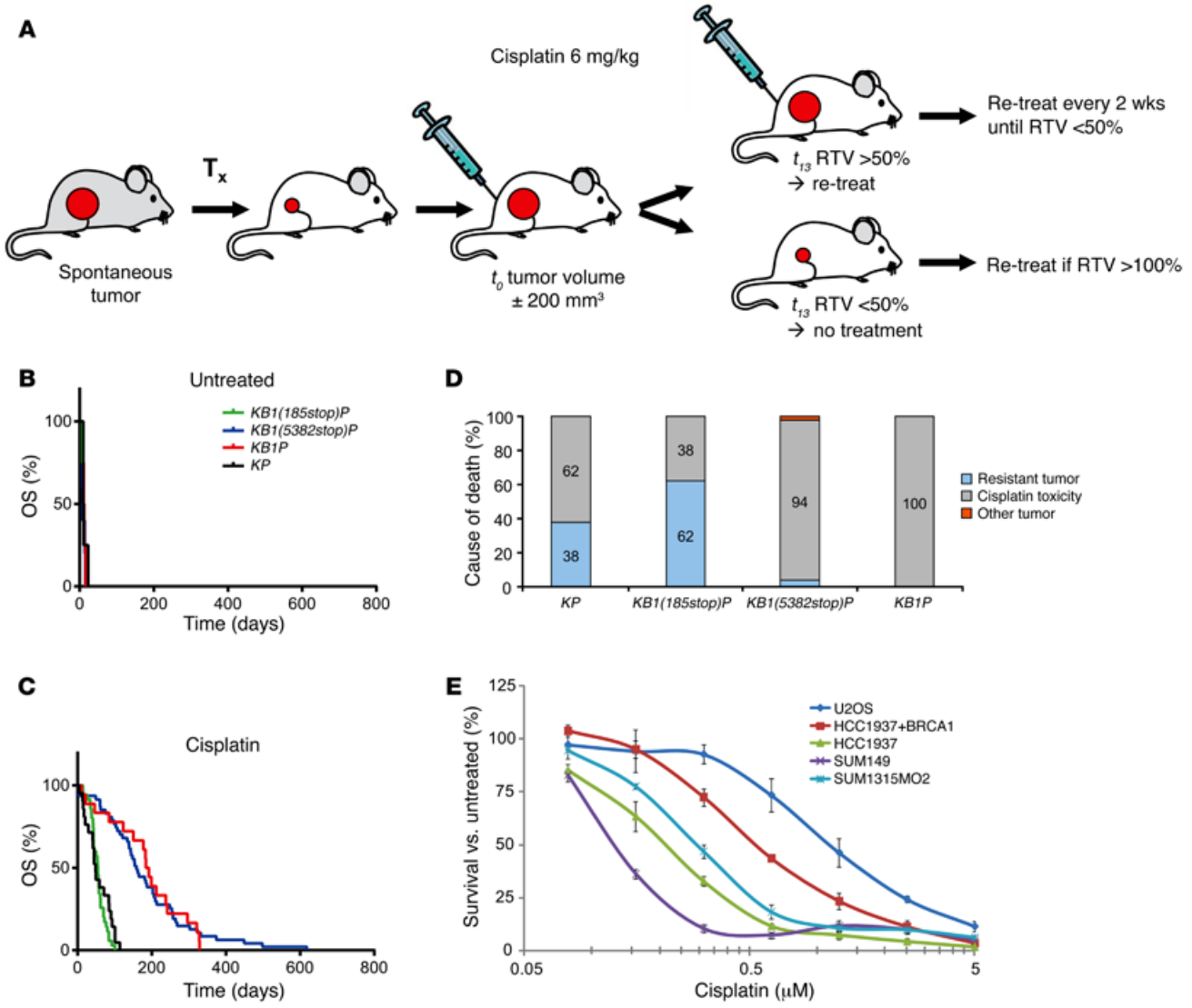

Figure 4. Poor cisplatin response of *KB1(185stop)P* mouse mammary tumors. (**A**) Schematic representation of cisplatin treatment schedule. t_0, start of treatment with 6 mg/kg cisplatin i.v. at a tumor volume of 200 mm³, corresponding to a relative tumor volume (RTV) of 100%. t_{13}, if the RTV on day 13 was ≥50%, the mice received an additional treatment that was repeated every 2 weeks until an RTV of ≤50% was observed. If the RTV at t_{13} was ≤50%, re-treatment was postponed until an RTV of >100% was observed. (**B**) OS curves of mice transplanted with *KB1(185stop)P*, *KB1(5382stop)P*, *KB1P*, or *KP* tumors without treatment. t_{50}, median OS. *KB1(185stop)P*: t_{50} = 15 days, n = 4 mice; *KB1(5382stop)P*: t_{50} = 8 days, n = 6 mice; *KB1P*: t_{50} = 12 days, n = 4 mice; *KP*: t_{50} = 11 days, n = 4 mice. (**C**) OS curves of mice transplanted as indicated in **B** after cisplatin treatment. *KB1(185stop)P*: t_{50} = 55 days, n = 35 mice; *KB1(5382stop)P*: t_{50} = 159 days, n = 47 mice; *KB1P*: t_{50} = 188 days, n = 18 mice; *KP*: t_{50} = 48 days, n = 21 mice. $P < 0.0001$, by log-rank test for *KB1(185stop)P* vs. *KB1(5382stop)P*; $P < 0.0001$, by log-rank test for *KB1(185stop)P* vs. *KB1P*; $P = 0.2550$ (NS), by log-rank test for *KB1(185stop)P* vs. *KP*; $P = 0.9696$ (NS), by log-rank test for *KB1(5382stop)P* vs. *KB1P*; $P < 0.0001$, by log-rank test for *KB1(5382stop)P* vs. *KP*; and $P < 0.0001$, by log-rank test for *KB1P* vs. *KP*. (**D**) Causes of death of tumor-bearing mice after treatment with cisplatin. The stacked bars indicate the percentage of mice that were sacrificed because of cisplatin-resistant mammary tumors, cisplatin-associated toxicity, or another (mesenteric) tumor. (**E**) Cisplatin sensitivity of various human *BRCA1*-mutated breast cancer cell lines, including SUM149PT (*BRCA1*^{2288del7}), SUM1315MO2 (*BRCA1*^{185delAG}), and HCC1937 (*BRCA1*^{5382insC}). The U2OS osteosarcoma and WT BRCA1–complemented HCC1937 cell lines served as BRCA1-proficient controls. The experiment was performed in quadruplicate. Error bars indicate SEM.

to cisplatin was significantly worse than that of *KB1(5382stop)P* tumors [Figure 4C; *KB1(185stop)P* vs. *KB1(5382stop)P*, $P < 0.0001$, log-rank test; Supplemental Figure 3, A–E]. The difference in response to cisplatin was even more pronounced when we compared the TFS of mice transplanted with *KB1(185stop)P* or *KB1(5382stop)P* mammary tumors (Supplemental Figure 3F).

To investigate whether these findings might also be relevant for human patients, we evaluated the cisplatin sensitivity of several human *BRCA1*-mutant breast cancer cell lines. These included the SUM1315MO2 and HCC1937 cell lines, which carry *BRCA1*^{185delAG} and *BRCA1*^{5382insC} mutations, respectively. In line with our observations in the mouse models, *BRCA1*^{185delAG}-mutant SUM-1315MO2 human breast cancer cells were less sensitive to cisplatin than were other *BRCA1*-mutated human breast cancer cell lines, including the *BRCA1*^{5382insC}-mutant HCC1937 cell line (Figure 4E). However, *BRCA1*^{185delAG}-mutant SUM1315MO2 cells were more sensitive to cisplatin than were BRCA1-proficient U2OS cells or WT *BRCA1*–complemented HCC1937 cells (Figure 4E).

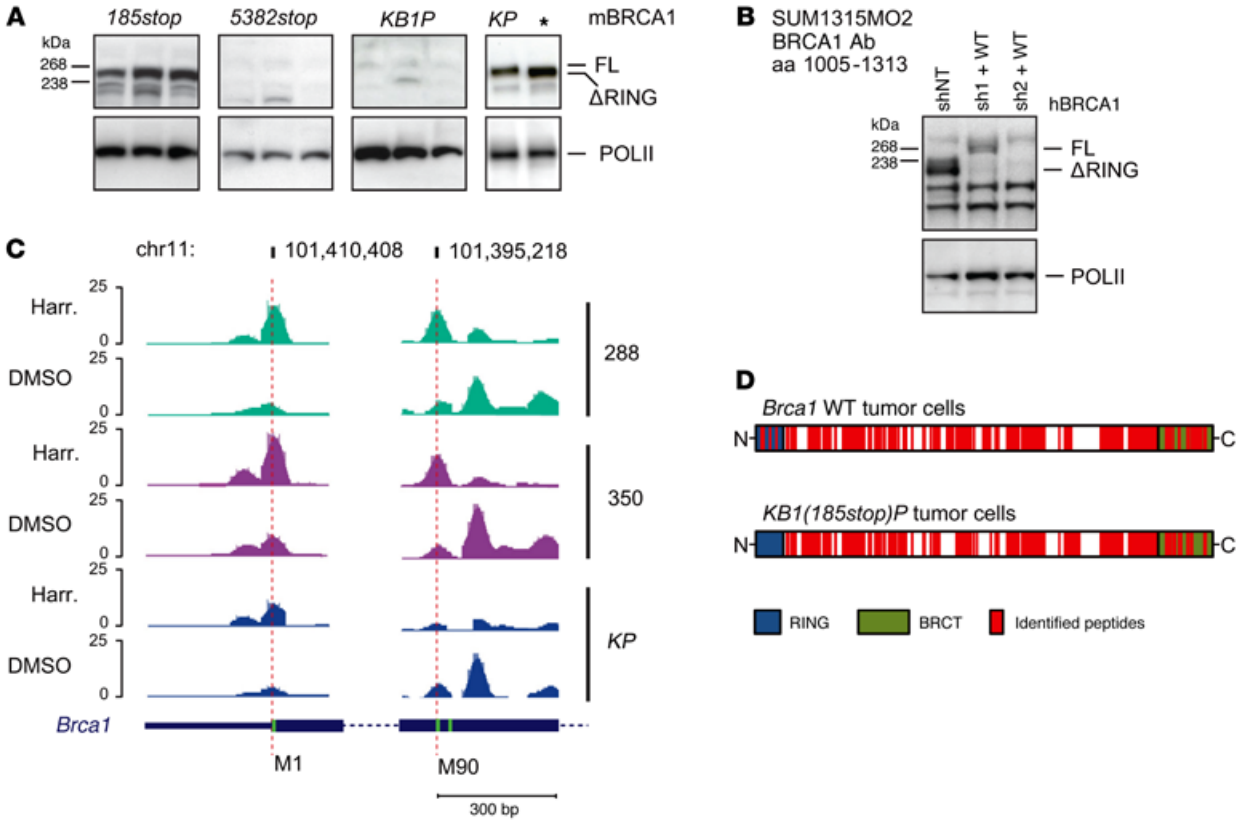

Figure 5. RING-less BRCA1 expression in mouse and human *BRCA1*^{185delAG} tumor cells. (**A**) BRCA1 protein expression in *KB1(185stop)P* mouse mammary tumors (left panel) compared with BRCA1-deficient *KB1(5382stop)P* and *KB1P* tumors (middle panels). A BRCA1-proficient *KP* tumor was used as a positive control (right panel). The asterisk in the far right panel indicates another *KB1(185stop)P* mouse mammary tumor. Expression of POLII was used as a loading control, and the positions of full-length (FL) and RING-less (ΔRING) BRCA1 and protein size markers are indicated. mBRCA1, murine BRCA1. (**B**) BRCA1 protein expression in the *BRCA1*^{185delAG}–mutant SUM1315MO2 human breast cancer cell line. As controls, SUM1315MO2 cells stably complemented with WT BRCA1 (WT) were depleted of endogenous BRCA1 by a *BRCA1* 3′-UTR–targeting shRNA (sh1) or depleted of both endogenous and ectopic BRCA1 using an shRNA targeting *BRCA1* exon 11 (sh2). shNT, NT shRNA. Expression of POLII was used as a loading control, and the positions of full-length and RING-less BRCA1 and protein size markers are indicated. hBRCA1, human BRCA1. (**C**) Ribosome profiling of *KB1(185stop)P* mammary tumor cell lines indicated a translation start at methionine 90. Ribosome footprint profile along *Brca1* exons 2 (containing methionine 1) and 6 (containing methionines 90 and 99) of 2 different *KB1(185stop)P* mouse mammary tumor cell lines (lines 280 and 350) and a *KP* control. Methionines are indicated in green. Harr., harringtonine; M1, methionine 1; M90, methionine 90. (**D**) Schematic representations of BRCA1 peptides identified by mass spectrometry in *Brca1* WT and *KB1(185stop)P* mouse mammary tumor cells.

Therapy resistance of mouse and human BRCA1^{185delAG} *tumor cells is not explained by genetic reversion or loss of 53BP1.* Given that BRCA1/2-deficient cell lines and ovarian tumors can become resistant to platinum compounds and olaparib through genetic reversion of the *BRCA1/2* mutation (57–60), we first checked whether the *Brca1*^{185stop} mutation was still present in platinum-resistant *KB1(185stop)P* tumors. Previously, we did not find any evidence for secondary *Brca1* mutations in therapy-resistant *KB1C61GP* tumors (43). Similarly, Sanger sequencing and melting-curve genotyping revealed that all cisplatin-resistant *KB1(185stop)P* tumors had retained the *Brca1*^{185stop} mutation (Supplemental Figure 4A and data not shown). On the basis of these results, we conclude that the observed platinum resistance in *KB1(185stop)P* mammary tumors is not caused by genetic reversion of the *Brca1*^{185stop} mutation. Furthermore, we were able to derive several cisplatin-resistant clones of the *BRCA1*-mutated human breast cancer cell line SUM1315MO2, all of which also retained the *BRCA1*^{185delAG} mutation (Supplemental Figure 4, B–D). In the absence of genetic reversion, loss of 53BP1 may also decrease the sensitivity of BRCA1-deficient mouse mammary tumors to olaparib and cisplatin (61). However, loss of 53BP1 does not explain the poor treatment response of the *KB1(185stop)P* mouse model, as platinum-resistant and treatment-naive tumors all showed abundant expression of 53BP1 (Supplemental Figure 4, D and E, and data not shown).

RING-less BRCA1 expression in mouse and human BRCA1^{185delAG} *tumor cells.* Since the response of *KB1(185stop)P* mouse mammary tumors to olaparib and cisplatin is similar to that of BRCA1-proficient *KP* tumors, we analyzed BRCA1 protein expression in *KB1(185stop)P* and *KB1(5382stop)P* mouse mammary tumors. Whereas *KB1(5382stop)P* tumors showed no detectable BRCA1 protein (Figure 5A), all *KB1(185stop)P* tumors showed expression of a nearly full-length BRCA1 protein, indicating translation initiation downstream from the *Brca1*^{185stop} mutation (Figure 5A). This finding suggests a discrepancy between the *Brca1*^{185stop} allele of our mouse model and the human *BRCA1*^{185delAG} allele, which was thought to express only a small N-terminal BRCA1 protein fragment of 38 aa (62).

We therefore checked BRCA1 protein expression levels in the SUM1315MO2 human breast cancer cell line, which carries the *BRCA1*^{185delAG} mutation. Remarkably, in *BRCA1*^{185delAG}-mutant SUM1315MO2 cells, BRCA1 immunoblotting also detected a large protein that could be completely depleted using *BRCA1*-specific shRNAs (Figure 5B). In contrast to the truncated BRCA1 formed by *KB1(185stop)P* tumor cells, the BRCA1 protein expressed by SUM1315MO2 cells was clearly smaller than full-length WT BRCA1, indicating the absence of a substantial part of the protein. In addition, we could not detect the truncated protein with a BRCA1 Ab that binds the extreme N-terminus of BRCA1 (aa 1–304; Supplemental Figure 5A). Together, these findings show that the *BRCA1*^{185delAG} mutation can lead to production of a mutant BRCA1-ΔRING protein, which is probably devoid of its N-terminal RING domain (aa 1–109).

Whether the truncated BRCA1 variant expressed by *KB1(185stop)P* tumor also lacks the RING domain cannot be deduced from the minimal size difference observed with full-length BRCA1. In the absence of Abs of sufficient quality to distinguish between full-length and RING-less mouse BRCA1 protein, we performed ribosome profiling of cell lines derived from treatment-naive *KB1(185stop)P* and *Brca1* WT *KP* mouse mammary tumors. We used harringtonine treatment to enrich for ribosomes at sites of translation initiation (63) and observed increased use of internal methionine 90 in *KB1(185stop)P* mouse mammary tumor cells compared with *KP* cells (Figure 5C). Since these data suggest that the nearly full-length BRCA1 protein expressed in *KB1(185stop)P* mouse mammary tumors also lacks the RING domain, mass spectrometric experiments were performed to verify the loss of the RING domain. BRCA1 protein was immunoprecipitated using an Ab raised against aa 1328–1812 (64) and analyzed after size selection by denaturing polyacrylamide gel electrophoresis. Whereas BRCA1-RING (aa 1–109) peptides were readily identified in WT BRCA1–expressing mouse tumor cells, they were not found in 2 different cell lines derived from *KB1(185stop)P* tumors (Figure 5D, Supplemental Figure 5B, and Supplemental Table 4). These data are compatible with the expression of RING-less BRCA1 in *KB1(185stop)P* cells. Given that even in WT BRCA1–expressing cells, not all possible RING peptides could be detected by mass spectrometry, the precise composition of BRCA1-ΔRING variants could not be determined (Figure 5D and Supplemental Figure 5B). However, analysis of the most N-terminal peptides identified supports a translation start at methionine 90, as suggested by ribosome profiling.

To test whether resistance in *KB1(185stop)P* tumors was due to increased expression of BRCA1-ΔRING, we analyzed *Brca1* mRNA and BRCA1-ΔRING protein levels. Although we found significantly increased *Brca1* mRNA levels in most platinum-resistant *KB1(185stop)P* tumors compared with levels in untreated tumors (Supplemental Figure 5C), we did not find a consistent concomitant increase in RING-less BRCA1 protein levels (Supplemental Figure 5D). Moreover, expression of RING-less BRCA1 protein was also not significantly increased in SUM1315MO2 clones that had been selected for increased resistance to cisplatin (Supplemental Figure 5A). These findings imply that upregulation of RING-less protein expression is not strictly required for *BRCA1*^{185delAG}-mutant tumor cells to become resistant to platinum therapy. Nevertheless, expression of RING-less BRCA1 distinguishes *KB1(185stop)P* tumors from *KB1P* tumors and most likely explains the poor response to HRD-targeted therapy.

DNA damage response in mouse and human BRCA1^{185delAG} *tumor cells*. The absence of genetic reversion of *Brca1* or loss of 53BP1 in platinum-resistant *KB1(185stop)P* tumors suggests that RING-less BRCA1 protein has residual activity in the cellular response to DNA DSBs. In line with our observation that *KB1(185stop)P* tumors showed some response to PARP1 inhibition, treatment with olaparib resulted in a DNA-damage increase similar to that seen in *KB1P* tumors (Figure 6A). However, we also found that the response to olaparib was eventually poor compared with that of *KB1P* tumors that were completely devoid of BRCA1 protein expression. To investigate whether RING-less BRCA1 protein has activity in DNA DSB repair via HR, we compared the ability to form RAD51 irradiation-induced foci (IRIF) in short-term tumor cell cultures derived from *KB1(185stop)P*, *KB1P*, and BRCA1-proficient *KP* tumors. As shown previously (43), we could readily detect RAD51 IRIF in short-term cultures of HR-proficient *KP* tumor cells, but not in HR-deficient *KB1P* tumor cells (Figure 6, B and C). *KB1(185stop)P* tumor cells were also able to form RAD51 IRIF (Figure 6, B and C). Despite the statistically significant difference, the data from the short-term ex vivo cell-culture experiments were quite variable. To gain further insight into the DNA damage response of *KB1(185stop)P* tumors, we continued our analysis in mouse mammary tumor–derived cell lines. In agreement with the loss of BRCA1 function we observed, *KB1(185stop)P* cell lines had a defect in DNA end resection, as replication protein A (RPA) accumulation at DSBs was impaired (Figure 6D). Indeed, *KB1(185stop)P* cell lines showed an initial deficiency in the repair of olaparib-induced DNA damage that was similar to that in *KB1P* cells (Figure 6E). Nevertheless, *KB1(185stop)* tumor cell lines showed RAD51 IRIF formation (Supplemental Figure 6A). In addition, human SUM-1315MO2 breast cancer cells — carrying the *BRCA1*^{185delAG} mutation — were also capable of forming RAD51 IRIF (Supplemental Figure 6B). Thus, both mouse and human *BRCA1*^{185delAG} tumor cells display HR activity in response to DNA damage, which could be the result of BRCA1-ΔRING expression.

To study whether the RING-less BRCA1 protein is functional in the DNA damage response, we checked for colocalization of BRCA1 with RAD51 after γ irradiation in cell lines derived from BRCA1-proficient, BRCA1-deficient, and *Brca1*^{185stop} mouse mammary tumors. While massive BRCA1/RAD51 colocalization was observed in BRCA1-proficient tumor cells, *Brca1*^{185stop} tumor cells showed fewer and smaller BRCA1/RAD51 IRIF (Supplemental Figure 6A and data not shown). In contrast, BRCA1-deficient *KB1P* B11 cells showed no BRCA1/RAD51 IRIF at all (Supplemental Figure 6A). These data suggest that the RING-less BRCA1 protein is partially functional in the response to DNA damage. This may explain why human and mouse *BRCA1*^{185delAG} tumor cells rapidly develop resistance to therapy that targets their HRD.

RING-less BRCA1 supports DNA repair via HR, resulting in reduced sensitivity of BRCA1^{185delAG} *tumor cells to PARP1 inhibition and cisplatin*. To test whether mutant RING-less BRCA1 protein is indeed functionally important for *BRCA1*^{185delAG} tumor cells, we performed *BRCA1*-knockdown experiments. Expression of RING-less BRCA1 in *BRCA1*^{185delAG}-mutant SUM1315MO2 cells was markedly reduced by transduction with lentiviruses encod-

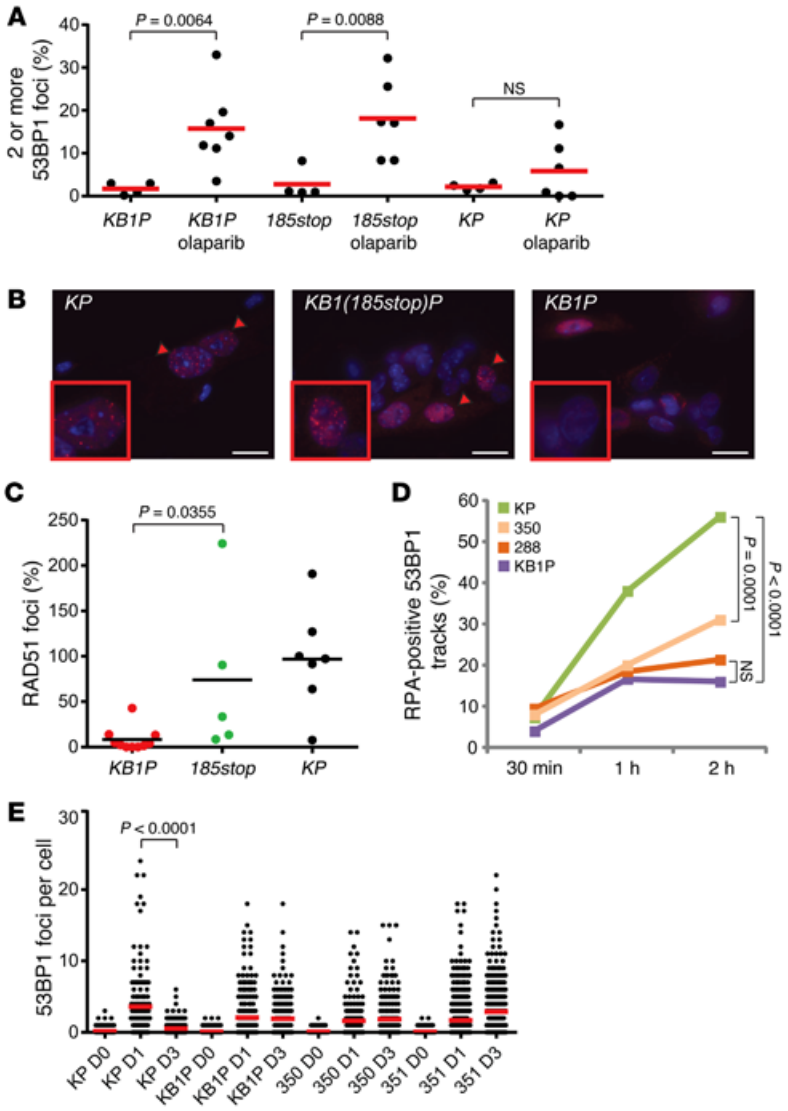

Figure 6. DNA damage response in mouse and human *BRCA1*^{185delAG} tumor cells. (**A**) Olaparib induced DNA damage in orthotopically transplanted *KB1(185stop)P* (*185stop*, *n* = 6), *KB1P* (*n* = 7), and *KP* (*n* = 6) tumors and nontreated controls (*n* = 4 for each genotype). Statistical significance was calculated using a 2-tailed, unpaired *t* test. (**B**) RAD51 IRIF in *KB1(185stop)P*, *KB1P*, and *KP* tumor cell suspensions. Nuclei (blue) with more than 10 RAD51 foci (red) are indicated with red arrowheads. Red outlined areas highlight single-cell zoom-in (zoom, ×63). Scale bars: 25 μm. (**C**) Quantification of RAD51 IRIF in *KB1(185stop)P* (*n* = 5), *KB1P* (*n* = 10), and *KP* (*n* = 7) tumors. Percentages were normalized to *KP*. Statistical significance was calculated using a 2-tailed, unpaired *t* test. (**D**) Accumulation of RPA at α tracks for 2 different *KB1(185stop)P* mouse mammary tumor cell lines (lines 350 and 351) and *KBP1* and *KP* controls. At least 100 53BP1 tracks were evaluated per time point in 2 to 3 replicate experiments, and statistical significance at 2 hours was calculated using Fisher's exact test. (**E**) Olaparib induced DNA damage in 2 different *KB1(185stop)P* mouse mammary tumor cell lines (lines 350 and 351) and *KB1P* and *KP* controls. Cells were cultured in normal medium (day 0 [D0]) or treated for 24 hours with 10 μM olaparib and either analyzed directly (D1) or after a 3-day recovery period (D3). Red bars indicate the mean number of 53BP1 foci in at least 120 cells, and data are representative of 2 independent experiments. Statistical significance was calculated using a 2-tailed, unpaired *t* test.

ing 2 independent shRNAs against human BRCA1 (Figure 7A; sh1 and sh2). Stable *BRCA1* knockdown significantly inhibited the proliferation of *BRCA1*^{185delAG} cells compared with cells transduced with a nontargeting (NT) shRNA (Supplemental Figure 7, A and B). In addition, we assessed the effect of *BRCA1* knockdown on the formation of RAD51 IRIF. The percentage of *BRCA1*^{185delAG}-mutant cells with RAD51 IRIF was significantly lower after *BRCA1* knockdown (Figure 7B and Supplemental Figure 7C). This was not a result of alterations in the cell-cycle distribution, as stable knockdown of *BRCA1* expression did not affect the number of *BRCA1*^{185delAG} cells in the S or G2 phase (Supplemental Figure 7D). To obtain direct evidence of the functional activity of RING-less BRCA1 proteins, we generated a series of N-terminal truncation mutants of human BRCA1. Western blot analysis of these mutants suggests that the main human RING-less BRCA1 protein is formed by alternative translation initiation at methionine 297 (Supplemental Figure 7E). Interestingly, BRCA1-M297 also appeared to be abundantly produced by cDNA constructs encoding BRCA1-M48 and BRCA1-M128 (Supplemental Figure 7E). All N-terminal truncation variants of BRCA1 tested were able to complement SUM1315MO2 *BRCA1*^{185delAG}-mutant cells depleted of endogenous BRCA1 expression by shRNAi in a clonal growth assay (Figure 7C and Supplemental Figure 7F). These data show that *BRCA1*^{185delAG} cells are dependent on expression of the RING-less BRCA1 protein, possibly through its function in the repair of DNA DSBs.

To further analyze the effects of RING-less BRCA1 expression on treatment response, we used mouse *KB1(185stop)P* tumor cells, which were much less dependent on RING-less BRCA1 for proliferation than were SUM1315MO2 cells (data not shown). *KB1(185stop)P* tumor cell lines showed varying levels of sensitivity to olaparib and cisplatin, which seemed to correlate to some extent with expression levels of RING-less BRCA1 protein (Supplemental Figure 8, A and B). Similar to SUM1315MO2 cells, *KB1(185stop)P* tumor cells also showed decreased RAD51 IRIF formation upon knockdown of *Brca1* expression (Supplemental Figure 8, C and D). As stable suppression of human or mouse BRCA1 expression was not sufficiently efficient for long-term cytotoxicity experiments (data not shown), we used CRISPR/Cas9 mutagenesis in *KB1(185stop)P* tumor cells to obtain

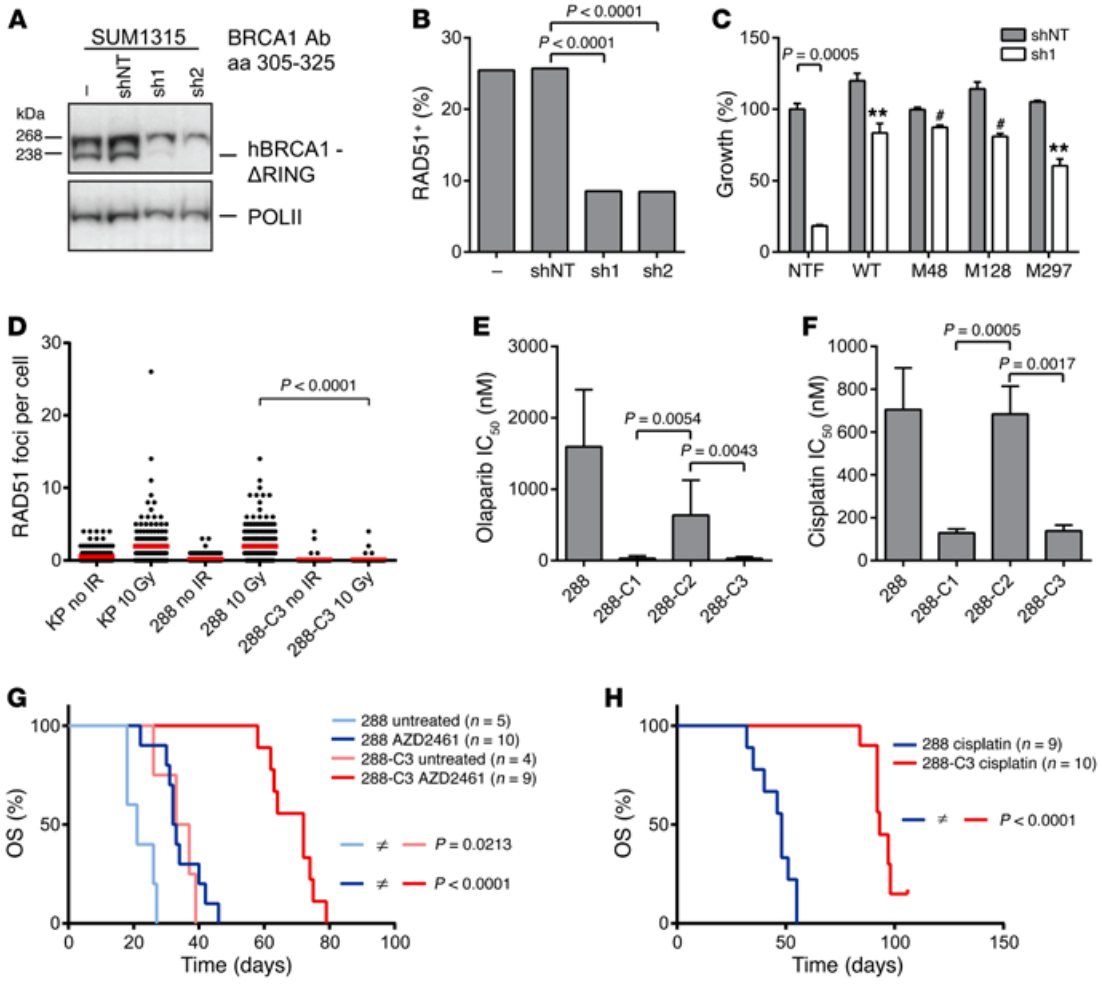

Figure 7. *BRCA1*^{185delAG} tumor cells are dependent on RING-less BRCA1 for proliferation, DNA damage signaling, and treatment response. (**A**) BRCA1 protein levels after *BRCA1* knockdown in *BRCA1*^{185delAG}-mutant SUM1315MO2 tumor cells. –, no shRNA. Expression of POLII was used as a loading control, and protein size markers are indicated. (**B**) Quantification of RAD51 IRIF–positive SUM1315MO2 cells after *BRCA1* knockdown as in **A**. The percentage of cells with 10 or more RAD51 foci was evaluated for at least 300 cells per condition. Statistical significance was calculated using Fisher's exact test, and results are representative of 2 independent experiments. (**C**) Complementation of SUM1315MO2 cells by stably transfected cDNA constructs expressing WT BRCA1 (WT) or BRCA1 N-terminal truncation variants (M48, M128, or M297). NTF, nontransfected control. Cells were assayed for clonal growth after transduction with the *BRCA1* 3′-UTR–targeting shRNA (sh1) or the NT shRNA (shNT) control. $P = 0.0005$ by 2-tailed, unpaired *t* test for NTF control shNT versus sh1. Significant complementation of proliferation is indicated by $^{**}P < 0.01$ or $^{\#}P < 0.0001$. Results shown are representative of 2 independent experiments. (**D**) RAD51 IRIF formation in *Brca1* WT (*KP*) cells, the *KB1(185stop)P* (288) cell line, and its *Brca1* deficient subclone C3 (288-C3). Cells were irradiated with 10 Gy, and RAD51 foci formation in S and G2 phases was compared with a nonirradiated control (no IR). Red bars indicate the mean number of foci in at least 116 EdU-positive cells. *P* value was determined using a 2-tailed, unpaired *t* test, and data are representative of 2 independent experiments. (**E** and **F**) IC_{50} values of *KB1(185stop)P* cell line 288 and subclones C1-3 for olaparib (**E**) and cisplatin (**F**). Error bars indicate the SD for 3 independent experiments. (**G** and **H**) OS of mice transplanted with *KB1(185stop)P* cell lines 288 and 288-C3 and treated with 100 mg/kg AZD2461 daily for 28 consecutive days (**G**) or with 6 mg/kg cisplatin on days 0 and 14 (**H**), or untreated (**G**). *P* values were calculated using the log-rank test.

evidence for the relevance of RING-less BRCA1 in therapy response. We targeted the BRCA1-BRCT–encoding region using a single-guide RNA (sgRNA) specific for exon 21 of *Brca1*. In 2 of 3 *KB1(185stop)P* clones analyzed (clones C1 and C3), frameshift mutations in exon 21 of the *Brca1*^{185stop} allele resulted in loss of RING-less BRCA1 protein expression (Supplemental Figure 9, A and B). Similar to *Brca1* knockdown, these frameshift mutations disrupted RAD51 IRIF formation (Figure 7D and data not shown). In addition, inactivation of RING-less BRCA1 resulted in dramatically increased sensitivity to both olaparib and cisplatin (Figure 7, E and F). These results were confirmed using another sgRNA targeting the Cas9 nuclease to exon 17 in the BRCA1-BRCT–encoding region of the *Brca1*^{185stop} allele (Supplemental Figure 9, C–F).

To investigate whether disruption of the *Brca1*^{185stop} allele also translates to a better treatment response in vivo, we performed orthotopic transplantation experiments in mice. The parental *KB1(185stop)P* tumor cells and their *Brca1*-knockout clone C3 grew into mammary tumors with a similar latency (data not shown), although untreated C3 tumors tended to proliferate at a somewhat slower rate once palpable (Supplemental Figure 10A). Strikingly, we also observed in vivo that inactivation of the *Brca1*^{185stop} allele rendered *KB1(185stop)P* tumor cells much more sensitive to PARP inhibition and cisplatin (Figure 7, G and H, and Supplemental Fig-

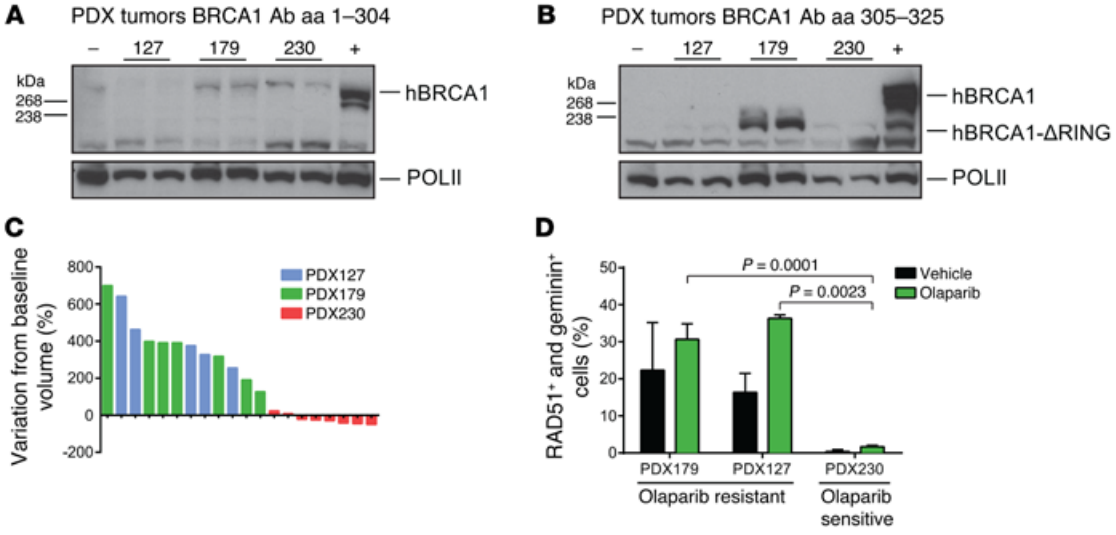

Figure 8. A RING-less BRCA1–expressing *BRCA1*^{185delAG} PDX model of breast cancer shows poor response to olaparib. (**A** and **B**) Western blot analysis of BRCA1 expression in 3 different *BRCA1*^{185delAG} PDX models of breast cancer and BRCA1-deficient (–) and BRCA1-proficient (+) controls, using the BRCA1 Abs MS110 (**A**; epitope: aa 1–304) and 9010 (**B**; epitope: aa 305–325). Expression of POLII was used as a loading control, and protein size markers are indicated. (**C**) Waterfall plot showing the olaparib response of individual PDX mammary tumors after 31 (PDX127, PDX230) or 33 (PDX179) days of treatment (50 mg/kg olaparib, i.p., 5 days/week). (**D**) Quantification of RAD51 foci in olaparib- or vehicle-treated *BRCA1*^{185delAG} PDX tumors. Percentages of S/G2-phase cells (geminin$^+$) with 5 or more RAD51 foci (RAD51$^+$) were determined on FFPE tumor samples for each PDX model. Error bars indicate the SD for 3 biological replicates, and *P* values were determined using a 2-tailed, unpaired *t* test.

ure 10, B and C). We used the PARP inhibitor AZD2461, which is a poor P-glycoprotein substrate, to avoid resistance caused by increased drug efflux (61). Mammary tumors derived from transplanted *KB1(185stop)P* cells only showed a moderate response to 28 days of treatment with AZD2461, with an increase of median survival from 21 to 32.5 days. In contrast, the median latency of tumors derived from the *Brca1*-knockout *KB1(185stop)P* clone C3 doubled from 35 to 72 days. Similarly, inactivation of the *Brca1*^{185stop} allele resulted in a much more durable response to cisplatin. Two doses of cisplatin increased the median latency period for *KB1(185stop)P* outgrowths to 48 days, whereas mice bearing C3 tumors showed an increase in median survival out to 93 days. Thus, expression of RING-less BRCA1 variants can indeed lead to decreased sensitivity to HRD-targeted therapy.

Decreased sensitivity of BRCA1^{185delAG} *PDX tumors expressing RING-less BRCA1 to PARP1 inhibition*. Although our data show that expression of RING-less BRCA1 can lead to HRD-targeted therapy resistance, it is not yet clear whether this is a relevant resistance mechanism in human cancer patients. To gain insight into the potential clinical relevance of RING-less BRCA1, we analyzed BRCA1 protein expression and olaparib response in 3 different *BRCA1*^{185delAG} patient-derived xenograft (PDX) models of breast cancer. In one of these models, PDX179, we detected putative RING-less BRCA1 protein (Figure 8, A and B). Similar to SUM1315MO2 cells, PDX179 tumors expressed a nearly full-length BRCA1 variant that was not detected by an Ab raised against the BRCA1 N-terminus. In the 2 other *BRCA1*^{185delAG} models, PDX127 and PDX230, we did not detect noticeable levels of RING-less BRCA1 expression. To investigate whether expression of RING-less BRCA1 would correlate with decreased sensitivity of *BRCA1*^{185delAG} tumors to PARP inhibition, we performed olaparib treatment studies for all 3 PDX models (Figure 8C and Supplemental Figure 11, A–C). In line with the data from the *KB1(185stop)P* mouse model, PDX179 did not respond well to olaparib (Figure 8C and Supplemental Figure 11B). Thus, residual activity of RING-less BRCA1 may cause resistance to PARP inhibition in human tumors as well. The data for PDX127 illustrate that also *BRCA1*^{185delAG} tumors with undetectable levels of (RING-less) BRCA1 expression may also show a poor response to treatment (Figure 8C and Supplemental Figure 11A), suggesting the existence of multiple mechanisms of resistance. Of note, similarly low expression levels of RING-less BRCA1 did not prevent regression of PDX230 tumors upon olaparib treatment (Figure 8C and Supplemental Figure 11C). We found no evidence of genetic reversion in any of the olaparib-resistant tumors (Figure 8, A and B, and data not shown). The results from the *BRCA1*^{185delAG} PDX tumors support the data from our mouse models and tissue culture experiments and warrant a careful evaluation of response data from *BRCA1*^{185delAG} breast and ovarian cancer patients treated with platinum drugs or PARP inhibitors.

Discussion

We have used genetically engineered mouse models mimicking the 2 most common *BRCA1* founder mutations, *BRCA1*^{185delAG} and *BRCA1*^{5382insC}, to study the effects of these mutations on tumor development and therapy response and resistance. While mice carrying the *Brca1*^{185stop} or *Brca1*^{5382stop} mutation develop similar types of mammary carcinomas, *Brca1*^{185stop} tumors respond significantly worse to HRD-targeted therapy than do *Brca1*^{5382stop} tumors and rapidly develop therapy resistance. It has previously been shown that secondary mutations in *BRCA1* can mediate resistance to platinum-based chemotherapy in *BRCA1*^{185delAG} ovarian carcinomas (59, 60). However, we could not detect genetic reversion of the *Brca1*^{185stop} mutation in any of the platinum-resistant *Brca1*^{185stop}

mouse mammary tumors. Also, in multiple cisplatin-resistant clones of the human *BRCA1*^{185delAG} breast cancer cell line SUM-1315MO2, no reversal of the mutation was found. Instead, we noticed that mouse and human *BRCA1*^{185delAG} tumor cells produced RING-less BRCA1 proteins, which are involved in the development of platinum and PARP inhibitor resistance through their activity in the DNA damage response.

A role for RING-less BRCA1 proteins in therapy response and resistance. While it was thus far thought that the *BRCA1*^{185delAG} frameshift mutation only leads to the formation of a small N-terminal protein of 38 aa, we detected nearly full-length, RING-less BRCA1 protein in *Brca1*^{185stop} mouse mammary tumors. This was not merely an artifact of our genetically engineered mouse model, since we could also detect RING-less BRCA1 in human breast cancer cells carrying the *BRCA1*^{185delAG} mutation.

Brca1^{185stop} tumors did not require secondary *Brca1* mutations to become resistant to PARP inhibition or cisplatin, because residual activity of the RING-less BRCA1 protein was already sufficient to withstand these types of targeted therapeutics. This finding extends the conclusions of our previous work with *Brca1*^{C61G} tumors, which expressed a full-length BRCA1 protein containing a missense mutation in the RING domain (43). Our data indicate that RING-less BRCA1 is not completely functional in HR, but that this protein still supports RAD51 IRIF formation. Thus, while insufficient for embryonic survival and tumor suppression, the residual activity of the RING-less BRCA1 protein can contribute to the rapid development of therapy resistance in *Brca1*^{185stop} tumors. Our data suggest that there is no strict requirement for upregulation or stabilization of RING-less BRCA1 protein levels for resistance to occur. In both human and mouse breast cancer cells, RING-less BRCA1 supported RAD51 IRIF formation, demonstrating its functional significance. Moreover, deletion of the *Brca1*^{185stop} allele rendered *KB1(185stop)P* tumor cells sensitive to cisplatin and PARP inhibition. To further investigate the potential relevance of our findings for human cancer patients, we analyzed 3 independent *BRCA1*^{185delAG} PDX models of breast cancer for expression of RING-less BRCA1 and response to PARP inhibition. In concordance with the data from our genetically engineered mouse models and the SUM1315MO2 cell line, a PDX model expressing RING-less BRCA1 showed progressive disease in the presence of the PARP inhibitor olaparib. Thus, human tumors expressing RING-less BRCA1 may also be resistant to HRD-targeted therapy. Although we detected no RING-less BRCA1 expression in another PDX model that showed resistance to olaparib, we found no evidence for genetic reversion of the *BRCA1*^{185delAG} mutation in any of the PDX tumors.

Why, then, are secondary *BRCA1* mutations still observed in therapy-resistant *BRCA1*^{185delAG} human ovarian carcinomas? One possibility is that these secondary *BRCA1* mutations are already present in rare cells of primary carcinomas, possibly because of genomic instability, and subsequently selected under the pressure of chemotherapy. This has been described before for chronic myeloid leukemia, in which *BCR-ABL* mutations that confer imatinib resistance are already present in a minority of tumor cells before exposure to the drug (65). In addition, the level of RING-less BRCA1 protein in untreated *BRCA1*^{185delAG} human ovarian carcinomas is currently unknown. There could be considerable intertumoral heterogeneity in both the presence (and abundance) of preexisting secondary *BRCA1* mutations and the expression levels of RING-less BRCA1 protein. Furthermore, we observed substantial differences among tumors in the levels of RING-less BRCA1 expression, which may also exist between *BRCA1*^{185delAG} breast and ovarian cancers. Genetic reversion might be the preferred mechanism of therapy resistance in tumors with preexisting secondary *BRCA1* mutations and weak or no expression of the RING-less BRCA1 protein.

The existence of RING-less BRCA1 proteins in mouse and human *BRCA1*^{185delAG} tumor cells appears to be the result of internal translation reinitiation at downstream start codons, as has previously been observed in transient transfection experiments with human *BRCA1* minigenes (66). Translation initiation at methionine 297 of human BRCA1 could also explain why *BRCA1*^{185delAG} mRNA is not degraded by NMD (66, 67). The mutant RING-less BRCA1 protein produced in our genetically engineered *Brca1*^{185stop} mouse model is somewhat larger than its human counterpart, most likely because of usage of the more upstream alternative start codon at methionine 90 in the mouse *Brca1* coding sequence.

Differences in therapy response between BRCA1 founder mutations. While patients with *BRCA1*-mutated ovarian cancer have a better prognosis after platinum-based chemotherapy than do nonmutation carriers (15–18), some heterogeneity in survival appears to exist among carriers of different *BRCA1* mutations (16). Survival of ovarian cancer patients carrying the *BRCA1*^{185delAG} mutation has been compared with that of *BRCA1*^{5382insC} patients, but, unfortunately, no conclusions could be drawn because of the small number of patients with a *BRCA1*^{5382insC} mutation (16). Our data indicate that the poor therapy response of *Brca1*^{185stop} mouse mammary tumors is mediated by residual activity of the RING-less BRCA1 protein. Therefore, we predict that RING-less BRCA1 expression may also have consequences for the clinical response of *BRCA1*^{185delAG} patients to DNA-damaging therapy.

Expression of a RING-less BRCA1 protein may not be limited to *BRCA1*^{185delAG} tumors, but could also occur in tumors carrying other truncating mutations in the N-terminus of BRCA1. Our data suggest that the presence of a RING-less BRCA1 protein in these tumors can serve as a marker to predict poor response to treatment with platinum or PARP inhibitors. PARP inhibitors are currently being tested in phase III clinical trials for *BRCA1/2*-associated breast cancers and approved for advanced *BRCA1/2*-associated ovarian cancers. Although pathogenic germline mutations in *BRCA1* or *BRCA2* are thus far the best predictors of PARP inhibitor sensitivity, it will be important to critically evaluate the treatment response of tumors with mutations affecting the N-terminus of BRCA1. This type of analysis will require large numbers of patients carrying specific *BRCA1* founder mutations and therefore remains a challenge for the future. Meanwhile, our genetically engineered and PDX mouse models offer ideal platforms for testing hypotheses on therapy response and resistance. Knowledge gained from these models could contribute to more accurate predictions of therapy responses of different *BRCA1* mutation carriers, help to prevent ineffective treatment, and lead to earlier development and implementation of alternative therapeutic agents.

Methods

Generation of Brca1^{185stop}- and Brca1^{5382stop}-mutant mice. Nonchemically modified deoxyribonucleotides (Sigma-Genosys) were used to introduce the *Brca1^{185stop}* (5′-ATGCAGAAAATCTTAGAGTAGGCGATCTGGTAAGTCAACA-3′) and *Brca1^{5382stop}* (5′-CAAGGCGATCCAGAGAATCAGGACCGGGAAAAGGTAAAGTC-3′) mutations into mESCs. The procedures for the introduction of oligonucleotides into mESCs, selection for G418-resistant colonies, and identification and purification of modified cells have been described previously (44–47). The resulting ESCs were injected into C57BL/6J blastocysts to produce chimeric males, which were mated with FVB females to generate *Brca1$^{+/185stop}$* and *Brca1$^{+/5382stop}$* mice. *Brca1$^{+/185stop}$* and *Brca1$^{+/5382stop}$* mice were bred with *K14-Cre Brca1$^{fl/fl}$ p53$^{fl/fl}$* (*KB1P*) animals (48) to generate *K14-Cre Brca1$^{185stop/fl}$ p53$^{fl/fl}$* [*KB1(185stop)P*] and *K14-Cre Brca1$^{5382stop/fl}$ p53$^{fl/fl}$* [*KB1(5382stop)P*] mice. Full details on the generation of the *Brca1^{185stop}* and *Brca1^{5382stop}* alleles and mouse genotyping are provided in the Supplemental Methods.

Embryo isolations. Timed matings were performed between *Brca1^{185stop}* or *Brca1^{5382stop}* heterozygous male and female mice. The impregnated females were sacrificed at various time points after conception, and their uteri were isolated in ice-cold PBS. The embryos were isolated by removing the muscular wall of the uterus, Reichert's membrane, and the visceral yolk sac. The visceral yolk sac was used for genotyping.

Orthotopic transplantations and drug interventions. Small fragments of mammary tumors from *KP*, *KB1P, KB1(185stop)P*, or *KB1(5382stop)P* mice were transplanted orthotopically into FVB:129/Ola F1 hybrid female mice as described previously (55). To generate mouse mammary tumors from *KB1(185stop)P* cell lines, 500,000 cells were transplanted into the fourth right mammary fat pad of 9-week-old female athymic nude RjOrl:NMRI-*Foxn1^{nu}/Foxn1^{nu}* mice (Janvier Labs) in 50 μl Matrigel (Corning) and PBS (1:1). When the tumor volume exceeded 200 mm^3, the mice were treated with the maximum tolerated dose (MTD) of cisplatin, olaparib, or AZD2461 (23, 55, 61). To study resistance, animals received additional doses of cisplatin when tumors grew back to a size of 200 mm^3. Animals were sacrificed when the tumor volume exceeded 1,500 mm^3 or when they became ill from drug toxicity.

The 3 PDX models used in this study were derived from PARP inhibitor–naive germline *BRCA1^{185delAG}* carriers presenting with hormone receptor–negative, HER2-negative, triple-negative breast cancers (TNBCs). The patient from whom PDX179 was derived had received cisplatin prior to tumor implantation into nude mice. PDX127 and PDX179 were derived from metastatic lesions, and PDX230 was derived from a primary tumor (additional clinical history is provided in the Supplemental Information). Tumors were s.c. implanted into 6-week-old female athymic nude HsdCpb:NMRI-*Foxn1^{nu}/Foxn1^{nu}* mice (Envigo). Animals were supplemented with 1 μmol/l 17β-estradiol (Sigma-Aldrich) in their drinking water. Upon xenograft growth, tumor tissue was reimplanted into recipient mice, which were randomized for olaparib or vehicle treatment, starting at tumor volumes between 50 and 500 mm^3. Treatment consisted of either vehicle (10% v/v DMSO in 10% w/v Kleptose (Roquette Laisa España) [HP-β-CD] in purified, deionized water) or 50 mg/kg olaparib in vehicle, administered i.p. 5 days per week.

Ribosome profiling of tumor cell lines. Ribosome-protected RNA fragments were isolated essentially as described before (63), and libraries were sequenced on an Illumina HiSeq 2000 system. A detailed protocol is described in the Supplemental Methods.

Mass spectrometric analysis of mouse RING-less BRCA1 protein. Immunoprecipitated BRCA1 was subjected to nanoflow liquid chromatography–tandem mass spectrometry (LC-MS/MS) on an 1100 Series Capillary LC System (Agilent Technologies) coupled to an LTQ Orbitrap XL Mass Spectrometer (Thermo Fisher Scientific). Detailed information on the experimental procedures is provided in the Supplemental Methods.

Sanger sequencing. Sequencing was done using the BigDye Terminator v3.1 Cycle Sequencing Kit (Applied Biosystems). Sequencing was performed on both genomic DNA and cDNA from tumors and spleens. Primer information is provided in the Supplemental Methods.

Array comparative genome hybridization and data analysis. Genomic DNA samples from tumors and spleens were labeled with the NimbleGen Dual-Color DNA Labeling Kit and hybridized to the NimbleGen 12-plex 135K full-genome mouse custom NKI array. Details of the analysis are described in the Supplemental Methods.

Clonogenic survival assays. Human and mouse cancer cell lines were plated onto 12-well plates at densities of 15,000 (SUM1315MO2, SUM149PT, HCC1937, and UWB.289.1); 6,000 (U2OS); and 600–1,000 (*KB1(185stop)P*) cells per well, respectively. For comparisons of *KB1(185stop)P, KP*, and *KB1P* cell lines, 1,000 *KB1(185stop)P* and *KP* cells and 3,000 *KB1P* B11 cells were plated onto 6-well plates. Twelve hours to one day after plating, a range of concentrations of cisplatin (Sigma-Aldrich or Mayne Pharma) in saline or olaparib (AZD2281; Selleck Chemicals or AstraZeneca) in DMSO was added to the cells. Cells were also treated with only saline or DMSO as the "no-drug control." Cells were allowed to grow in the presence of the drug for 7 days and stained with 0.1% to 1% crystal violet. Clonogenic survival was determined by measuring the absorbance of crystal violet at 590 to 595 nm. Full details on cell culture conditions are provided in the Supplemental Methods.

BRCA1- and Brca1-knockdown experiments. Cells were transduced with pLKO-puro shRNA viruses (TRC library clones; Thermo Scientific Open Biosystems) targeting human *BRCA1* or mouse *Brca1* or an NT control. After puromycin selection, cells were assayed for γ irradiation–induced DNA repair foci or seeded for clonal growth. SUM1315MO2 cells were incubated with CellTiter-Blue (Promega) or fixed and stained with crystal violet after 2 weeks of clonal growth, and fluorescence or absorbance were measured. Full details are provided in the Supplemental Methods.

CRISPR/Cas9-mediated inactivation of the Brca1^{185stop} allele. CRISPR/Cas9 mutagenesis was performed as described previously (68). Briefly, *KB1(185stop)P* mouse mammary tumor cells were transiently transfected with a modified pX330 CRISPR/Cas9 plasmid (Addgene plasmid 42230) containing a puromycin resistance marker and targeting the BRCT-encoding region of *Brca1*. After 2 days of puromycin selection (1.8 μg/ml), cells were seeded at clonal density, and colonies were selected for further analyses and experiments. Full details are provided in the Supplemental Methods.

Immunoblotting. Tumor protein lysates were made by using a microhomogenizer and radioimmunoprecipitation assay (RIPA) lysis buffer (50 mM Tris, pH 8.0, 150 mM NaCl, 0.1% SDS, 0.1% deoxycholate, 1% NP40), complemented with 2× Complete Protease Inhibitor Cocktail (Roche) and Pefabloc (Roche; 1 mg/ml). Following homogenization on ice, tumor lysates were kept on ice for 30 minutes. After a

short spin, protein concentrations were determined with the BCA Protein Assay Kit (Pierce, Thermo Fisher Scientific), and samples were prepared for gel electrophoresis. Western blotting was performed as described previously (69).

Immunofluorescence analyses and IHC. Immunofluorescence and IHC were essentially performed as described before (43, 70). For ex vivo analysis of RAD51 foci formation, cells from cryopreserved tumors were grown on glass coverslips for 36 to 48 hours, γ irradiated with 10 Gy, and fixed 6 hours later in 2% paraformaldehyde. To quantify RAD51 foci in single tumor cells, 150–200 cells per condition were counted blindly. Cells were scored as RAD51 positive if they had more than 10 RAD51-positive dots per nucleus. For quantification of 53BP1 foci in formalin-fixed, paraffin-embedded (FFPE) sections of olaparib-treated mouse mammary tumors, at least 200 cells were counted using ImageJ software (NIH). Recruitment of RPA to 53BP1-positive DNA DSBs was analyzed using α particle irradiation through the bottom of a Mylar dish, as described by Stap et al. (71). A list of Abs and full procedures for immunohistochemical and immunofluorescence assays are provided in the Supplemental Methods.

aCGH data. aCGH data generated in this study have been deposited in the NCBI's Gene Expression Omnibus (GEO) database (GEO GSE43997).

Statistics. Statistical analyses were performed using GraphPad Prism 6 (GraphPad Software). Kaplan-Meier survival curves were compared using the log-rank test, contingency tables were compared using Fisher's exact test, and other data were compared using 2-tailed *t* tests. A *P* value of less than 0.05 was considered significant, except when Bonferroni's correction was applied to correct the significance threshold for multiple testing ($P < 0.025$ for Figure 6D, Figure 7, B, E, and F, Figure 8D, Supplemental Figure 7B, Supplemental Figure 9, E and F, and $P < 0.01$ for Supplemental Table 3D).

Study approval. All experiments involving genetically engineered mouse models complied with local and international regulations and ethics guidelines and were approved by the IACUC of the Netherlands Cancer Institute (DEC-NKI). For PDX tumors, patients' consent for tumor use in animals was obtained under a protocol approved by the Vall d'Hebron Hospital Clinical Investigation Ethics Committee. Mice were maintained and treated in accordance with institutional guidelines, and experiments were approved by the IACUC of the Vall d'Hebron Institute of Research (VHIR Animal Use Committee).

Author contributions

RD, TT, PB, and JJ designed the study. RD, KKD, HvdG, IvdH, IB, CC, DC, MCB, UB, ES, EvdB, EW, MP, FLP, LvD, DHWD, and PB performed experiments. RD, KKD, IB, CC, CK, SK, FLP, RE, DHWD, and PB analyzed data. RD, SR, MvdV, JAAD, DCvG, RA, JB, VS, TT, PB, and JJ supervised experiments. RD, PB, and JJ wrote the manuscript, with input and scientific advice from VS and TT.

Acknowledgments

We thank the personnel of the NKI animal facility and the NKI Mouse Cancer Clinic transgenic facility and preclinical intervention unit for excellent help with the mouse experiments; the NKI animal pathology, digital microscopy, and genomics core facilities for expert help; M. O'Connor (AstraZeneca) for providing olaparib; R. Kanaar and A. Zelensky (Erasmus MC, Rotterdam, Netherlands) for the RAD51 Ab and advice; R.I. Drapkin (University of Pennsylvania, Philadelphia, Pennsylvania, USA) for the polyclonal mouse BRCA1 Ab; M. Schutte (Erasmus MC) and Paul Andreassen (Cincinnati Children's Research Foundation, Cincinnati, Ohio, USA) for human breast cancer cell lines; M. Aarts, M. Dekker, S. de Vries, T. Harmsen, B. van den Broek, M. Barazas, P. ter Brugge, K. Rooijers (all from the NKI), and Y.H. Ibrahim and M. Guzmán (from the Vall d'Hebron Institute of Oncology) for expert help and technical assistance. This work was supported by grants from the Dutch Cancer Society (NKI 2007-3772, to JJ, SR, and J. Schellens [all from the NKI]; NKI 2008-4116, to JJ and PB; NKI 2012-5220, to SR, and JJ; EMCR 2008-4045, to DCvG; NKI 2015-7877, to PB, JJ, and MPG Vreeswijk [Leiden University Medical Center, Leiden, The Netherlands]); the Netherlands Organization for Scientific Research (NWO) (Cancer Genomics Netherlands [CGCNL], Cancer Systems Biology Center [CSBC], Netherlands Genomic Initiative Zenith 93512009, to JJ, and NWO VICI 91814643, to JJ); the European Union Seventh Framework Programme (EurocanPlatform project 260791 and DDResponse project 259893); the European Research Council (ERC) (CombatCancer ERC Synergy Project); a Ride for the Roses Cancer Research Grant (EMCR 2011-5030, to DvG); the Howard Hughes Medical Institute (to TT); the National Cancer Institute (NCI), NIH (R01 CA125636, to TT); and the NCI, NIH Chromosome Metabolism and Cancer Training Grant (T32 CA009657-21, to KD). KKD is a Thomsen Breast Cancer Fellow. Further support was provided by the Netherlands Proteomics Centre (NPC) and the Mouse Clinic for Cancer and Aging (MCCA), financed by the NWO as part of the National Roadmap for Large-Scale Research Facilities. Work at the Vall D'Hebron Institute of Oncology was supported by the Instituto de Salud Carlos III (PI12/02606, to JB) and the Asociación Española Contra el Cáncer (to CC).

Address correspondence to: Jos Jonkers or Peter Bouwman, Plesmanlaan 121, 1066 CX Amsterdam, Netherlands. Phone: 0031.20.5122000; E-mail: j.jonkers@nki.nl (J. Jonkers), p.bouwman@nki.nl (P. Bouwman). Or to: Toshiyasu Taniguchi, 1100 Fairview Ave. N., C1-015 Seattle, Washington 98109-1024, USA. Phone: 206.667.7283; E-mail: ttaniguc@fhcrc.org.

1. DeSantis C, Siegel R, Bandi P, Jemal A. Breast cancer statistics, 2011. *CA Cancer J Clin*. 2011;61(6):409–418.
2. Rahman N, Stratton MR. The genetics of breast cancer susceptibility. *Annu Rev Genet*. 1998;32:95–121.
3. Smith TM, et al. Complete genomic sequence and analysis of 117 kb of human DNA containing the gene BRCA1. *Genome Res*. 1996;6(11):1029–1049.
4. Conti E, Izaurralde E. Nonsense-mediated mRNA decay: molecular insights and mechanistic variations across species. *Curr Opin Cell Biol*. 2005;17(3):316–325.
5. Lejeune F, Maquat LE. Mechanistic links between nonsense-mediated mRNA decay and pre-mRNA splicing in mammalian cells. *Curr Opin Cell Biol*. 2005;17(3):309–315.
6. Phelan CM, et al. A low frequency of non-founder BRCA1 mutations in Ashkenazi Jewish breast-ovarian cancer families. *Hum Mutat*. 2002;20(5):352–357.
7. Struewing JP, et al. The carrier frequency of the BRCA1 185delAG mutation is approximately 1 percent in Ashkenazi Jewish individuals. *Nat Genet*. 1995;11(2):198–200.
8. Roa BB, Boyd AA, Volcik K, Richards CS. Ashkenazi Jewish population frequencies for common mutations in BRCA1 and BRCA2. *Nat Genet*. 1996;14(2):185–187.
9. Moslehi R, et al. BRCA1 and BRCA2 muta-

tion analysis of 208 Ashkenazi Jewish women with ovarian cancer. *Am J Hum Genet*. 2000;66(4):1259–1272.
10. Frank TS, et al. Clinical characteristics of individuals with germline mutations in BRCA1 and BRCA2: analysis of 10,000 individuals. *J Clin Oncol*. 2002;20(6):1480–1490.
11. Levy-Lahad E, Friedman E. Cancer risks among BRCA1 and BRCA2 mutation carriers. *Br J Cancer*. 2007;96(1):11–15.
12. Venkitaraman AR. Cancer suppression by the chromosome custodians, BRCA1 and BRCA2. *Science*. 2014;343(6178):1470–1475.
13. Prakash R, Zhang Y, Feng W, Jasin M. Homologous recombination and human health: the roles of BRCA1, BRCA2, and associated proteins. *Cold Spring Harb Perspect Biol*. 2015;7(4):a016600.
14. Bhattacharyya A, Ear US, Koller BH, Weichselbaum RR, Bishop DK. The breast cancer susceptibility gene BRCA1 is required for subnuclear assembly of Rad51 and survival following treatment with the DNA cross-linking agent cisplatin. *J Biol Chem*. 2000;275(31):23899–23903.
15. Boyd J, et al. Clinicopathologic features of BRCA-linked and sporadic ovarian cancer. *JAMA*. 2000;283(17):2260–2265.
16. Ben David Y, et al. Effect of BRCA mutations on the length of survival in epithelial ovarian tumors. *J Clin Oncol*. 2002;20(2):463–466.
17. Foulkes WD. BRCA1 and BRCA2: chemosensitivity, treatment outcomes and prognosis. *Fam Cancer*. 2006;5(2):135–142.
18. Chetrit A, Hirsh-Yechezkel G, Ben-David Y, Lubin F, Friedman E, Sadetzki S. Effect of BRCA1/2 mutations on long-term survival of patients with invasive ovarian cancer: the national Israeli study of ovarian cancer. *J Clin Oncol*. 2008;26(1):20–25.
19. Byrski T, et al. Pathologic complete response rates in young women with BRCA1-positive breast cancers after neoadjuvant chemotherapy. *J Clin Oncol*. 2010;28(3):375–379.
20. Vollebergh MA, et al. An aCGH classifier derived from BRCA1-mutated breast cancer and benefit of high-dose platinum-based chemotherapy in HER2-negative breast cancer patients. *Ann Oncol*. 2011;22(7):1561–1570.
21. Bryant HE, et al. Specific killing of BRCA2-deficient tumours with inhibitors of poly(ADP-ribose) polymerase. *Nature*. 2005;434(7035):913–917.
22. Farmer H, et al. Targeting the DNA repair defect in BRCA mutant cells as a therapeutic strategy. *Nature*. 2005;434(7035):917–921.
23. Rottenberg S, et al. High sensitivity of BRCA1-deficient mammary tumors to the PARP inhibitor AZD2281 alone and in combination with platinum drugs. *Proc Natl Acad Sci USA*. 2008;105(44):17079–17084.
24. Audeh MW, et al. Oral poly(ADP-ribose) polymerase inhibitor olaparib in patients with BRCA1 or BRCA2 mutations and recurrent ovarian cancer: a proof-of-concept trial. *Lancet*. 2010;376(9737):245–251.
25. Fong PC, et al. Inhibition of poly(ADP-ribose) polymerase in tumors from BRCA mutation carriers. *N Engl J Med*. 2009;361(2):123–134.
26. Fong PC, et al. Poly(ADP)-ribose polymerase inhibition: frequent durable responses in BRCA carrier ovarian cancer correlating with platinum-free interval. *J Clin Oncol*. 2010;28(15):2512–2519.
27. Gelmon KA, et al. Olaparib in patients with recurrent high-grade serous or poorly differentiated ovarian carcinoma or triple-negative breast cancer: a phase 2, multicentre, open-label, non-randomised study. *Lancet Oncol*. 2011;12(9):852–861.
28. Tutt A, et al. Oral poly(ADP-ribose) polymerase inhibitor olaparib in patients with BRCA1 or BRCA2 mutations and advanced breast cancer: a proof-of-concept trial. *Lancet*. 2010;376(9737):235–244.
29. Ledermann J, et al. Olaparib maintenance therapy in patients with platinum-sensitive relapsed serous ovarian cancer: a preplanned retrospective analysis of outcomes by BRCA status in a randomised phase 2 trial. *Lancet Oncol*. 2014;15(8):852–861.
30. Tewari KS, Eskander RN, Monk BJ. Development of olaparib for BRCA-deficient recurrent epithelial ovarian cancer. *Clin Cancer Res*. 2015;21(17):3829–3835.
31. Huen MS, Sy SM, Chen J. BRCA1 and its toolbox for the maintenance of genome integrity. *Nat Rev Mol Cell Biol*. 2010;11(2):138–148.
32. Mallery DL, Vandenberg CJ, Hiom K. Activation of the E3 ligase function of the BRCA1/BARD1 complex by polyubiquitin chains. *EMBO J*. 2002;21(24):6755–6762.
33. Xia Y, Pao GM, Chen HW, Verma IM, Hunter T. Enhancement of BRCA1 E3 ubiquitin ligase activity through direct interaction with the BARD1 protein. *J Biol Chem*. 2003;278(7):5255–5263.
34. Morris JR, Solomon E. BRCA1 : BARD1 induces the formation of conjugated ubiquitin structures, dependent on K6 of ubiquitin, in cells during DNA replication and repair. *Hum Mol Genet*. 2004;13(8):807–817.
35. Shabbeer S, et al. BRCA1 targets G2/M cell cycle proteins for ubiquitination and proteasomal degradation. *Oncogene*. 2013;32(42):5005–5016.
36. Scully R, et al. BRCA1 is a component of the RNA polymerase II holoenzyme. *Proc Natl Acad Sci USA*. 1997;94(11):5605–5610.
37. Scully R, et al. Association of BRCA1 with Rad51 in mitotic and meiotic cells. *Cell*. 1997;88(2):265–275.
38. Anderson SF, Schlegel BP, Nakajima T, Wolpin ES, Parvin JD. BRCA1 protein is linked to the RNA polymerase II holoenzyme complex via RNA helicase A. *Nat Genet*. 1998;19(3):254–256.
39. Bochar DA, et al. BRCA1 is associated with a human SWI/SNF-related complex: linking chromatin remodeling to breast cancer. *Cell*. 2000;102(2):257–265.
40. Yarden RI, Brody LC. BRCA1 interacts with components of the histone deacetylase complex. *Proc Natl Acad Sci USA*. 1999;96(9):4983–4988.
41. Patel KJ, Crossan GP, Hodskinson MR. "Ring-fencing" BRCA1 tumor suppressor activity. *Cancer Cell*. 2011;20(6):693–695.
42. Shakya R, et al. BRCA1 tumor suppression depends on BRCT phosphoprotein binding, but not its E3 ligase activity. *Science*. 2011;334(6055):525–528.
43. Drost R, et al. BRCA1 RING function is essential for tumor suppression but dispensable for therapy resistance. *Cancer Cell*. 2011;20(6):797–809.
44. Dekker M, Brouwers C, te Riele H. Targeted gene modification in mismatch-repair-deficient embryonic stem cells by single-stranded DNA oligonucleotides. *Nucleic Acids Res*. 2003;31(6):e27.
45. Dekker M, et al. Effective oligonucleotide-mediated gene disruption in ES cells lacking the mismatch repair protein MSH3. *Gene Ther*. 2006;13(8):686–694.
46. Dekker M, et al. Transient suppression of MLH1 allows effective single-nucleotide substitution by single-stranded DNA oligonucleotides. *Mutat Res*. 2011;715(1-2):52–60.
47. Aarts M, Dekker M, de Vries S, van der Wal A, te Riele H. Generation of a mouse mutant by oligonucleotide-mediated gene modification in ES cells. *Nucleic Acids Res*. 2006;34(21):e147.
48. Liu X, et al. Somatic loss of BRCA1 and p53 in mice induces mammary tumors with features of human BRCA1-mutated basal-like breast cancer. *Proc Natl Acad Sci USA*. 2007;104(29):12111–12116.
49. Lakhani SR, et al. The pathology of familial breast cancer: predictive value of immunohistochemical markers estrogen receptor, progesterone receptor, HER-2, and p53 in patients with mutations in BRCA1 and BRCA2. *J Clin Oncol*. 2002;20(9):2310–2318.
50. Tirkkonen M, et al. Distinct somatic genetic changes associated with tumor progression in carriers of BRCA1 and BRCA2 germ-line mutations. *Cancer Res*. 1997;57(7):1222–1227.
51. Holstege H, et al. Cross-species comparison of aCGH data from mouse and human BRCA1- and BRCA2-mutated breast cancers. *BMC Cancer*. 2010;10:455.
52. Klijn C, et al. Identification of cancer genes using a statistical framework for multiexperiment analysis of nondiscretized array CGH data. *Nucleic Acids Res*. 2008;36(2):e13.
53. de Ronde JJ, et al. KC-SMARTR: An R package for detection of statistically significant aberrations in multi-experiment aCGH data. *BMC Res Notes*. 2010;3:298.
54. Pajic M, et al. Tumor-initiating cells are not enriched in cisplatin-surviving BRCA1;p53-deficient mammary tumor cells in vivo. *Cell Cycle*. 2010;9(18):3780–3791.
55. Rottenberg S, et al. Selective induction of chemotherapy resistance of mammary tumors in a conditional mouse model for hereditary breast cancer. *Proc Natl Acad Sci USA*. 2007;104(29):12117–12122.
56. Silver DP, et al. Efficacy of neoadjuvant Cisplatin in triple-negative breast cancer. *J Clin Oncol*. 2010;28(7):1145–1153.
57. Edwards SL, et al. Resistance to therapy caused by intragenic deletion in BRCA2. *Nature*. 2008;451(7182):1111–1115.
58. Sakai W, et al. Secondary mutations as a mechanism of cisplatin resistance in BRCA2-mutated cancers. *Nature*. 2008;451(7182):1116–1120.
59. Swisher EM, Sakai W, Karlan BY, Wurz K, Urban N, Taniguchi T. Secondary BRCA1 mutations in

BRCA1-mutated ovarian carcinomas with platinum resistance. *Cancer Res*. 2008;68(8):2581–2586.
60. Norquist B, et al. Secondary somatic mutations restoring BRCA1/2 predict chemotherapy resistance in hereditary ovarian carcinomas. *J Clin Oncol*. 2011;29(22):3008–3015.
61. Jaspers JE, et al. Loss of 53BP1 causes PARP inhibitor resistance in Brca1-mutated mouse mammary tumors. *Cancer Discov*. 2013;3(1):68–81.
62. Elstrodt F, et al. BRCA1 mutation analysis of 41 human breast cancer cell lines reveals three new deleterious mutants. *Cancer Res*. 2006;66(1):41–45.
63. Ingolia NT, Lareau LF, Weissman JS. Ribosome profiling of mouse embryonic stem cells reveals the complexity and dynamics of mammalian proteomes. *Cell*. 2011;147(4):789–802.
64. Sotiropoulou PA, et al. BRCA1 deficiency in skin epidermis leads to selective loss of hair follicle stem cells and their progeny. *Genes Dev*. 2013;27(1):39–51.
65. Roche-Lestienne C, et al. Several types of mutations of the Abl gene can be found in chronic myeloid leukemia patients resistant to STI571, and they can pre-exist to the onset of treatment. *Blood*. 2002;100(3):1014–1018.
66. Buisson M, Anczuków O, Zetoune AB, Ware MD, Mazoyer S. The 185delAG mutation (c.68_69delAG) in the BRCA1 gene triggers translation reinitiation at a downstream AUG codon. *Hum Mutat*. 2006;27(10):1024–1029.
67. Perrin-Vidoz L, Sinilnikova OM, Stoppa-Lyonnet D, Lenoir GM, Mazoyer S. The nonsense-mediated mRNA decay pathway triggers degradation of most BRCA1 mRNAs bearing premature termination codons. *Hum Mol Genet*. 2002;11(23):2805–2814.
68. Cong L, et al. Multiplex genome engineering using CRISPR/Cas systems. *Science*. 2013;339(6121):819–823.
69. Bouwman P, et al. A high-throughput functional complementation assay for classification of BRCA1 missense variants. *Cancer Discov*. 2013;3(10):1142–1155.
70. Bouwman P, et al. 53BP1 loss rescues BRCA1 deficiency and is associated with triple-negative and BRCA-mutated breast cancers. *Nat Struct Mol Biol*. 2010;17(6):688–695.
71. Stap J, et al. Induction of linear tracks of DNA double-strand breaks by alpha-particle irradiation of cells. *Nat Methods*. 2008;5(3):261–266.